NASA/TP—1999–208640

The SERTS–97 Rocket Experiment to Study Activity on the Sun: Flight 36.167–GS on 1997 November 18

Marvin Swartz, Charles E. Condor, Joseph M. Davila, J. Patrick Haas, Stuart D. Jordan, David L. Linard, Joseph J. Miko, I.Carol Nash, Joseph Novello, Leslie J. Payne, Thomas B. Plummer, Roger J. Thomas, Larry A. White, Jeffrey W. Brosius, and William T. Thompson

February 1999

The NASA STI Program Office … in Profile

Since its founding, NASA has been dedicated to the advancement of aeronautics and space science. The NASA Scientific and Technical Information (STI) Program Office plays a key part in helping NASA maintain this important role.

The NASA STI Program Office is operated by Langley Research Center, the lead center for NASA's scientific and technical information. The NASA STI Program Office provides access to the NASA STI Database, the largest collection of aeronautical and space science STI in the world. The Program Office is also NASA's institutional mechanism for disseminating the results of its research and development activities. These results are published by NASA in the NASA STI Report Series, which includes the following report types:

- TECHNICAL PUBLICATION. Reports of completed research or a major significant phase of research that present the results of NASA programs and include extensive data or theoretical analysis. Includes compilations of significant scientific and technical data and information deemed to be of continuing reference value. NASA's counterpart of peer-reviewed formal professional papers but has less stringent limitations on manuscript length and extent of graphic presentations.
- TECHNICAL MEMORANDUM. Scientific and technical findings that are preliminary or of specialized interest, e.g., quick release reports, working papers, and bibliographies that contain minimal annotation. Does not contain extensive analysis.
- CONTRACTOR REPORT. Scientific and technical findings by NASA-sponsored contractors and grantees.
- CONFERENCE PUBLICATION. Collected papers from scientific and technical conferences, symposia, seminars, or other meetings sponsored or cosponsored by NASA.
- SPECIAL PUBLICATION. Scientific, technical, or historical information from NASA programs, projects, and mission, often concerned with subjects having substantial public interest.
- TECHNICAL TRANSLATION. English-language translations of foreign scientific and technical material pertinent to NASA's mission.

Specialized services that complement the STI Program Office's diverse offerings include creating custom thesauri, building customized databases, organizing and publishing research results . . . even providing videos.

For more information about the NASA STI Program Office, see the following:

- Access the NASA STI Program Home Page at http://www.sti.nasa.gov/STI-homepage.html
- E-mail your question via the Internet to help@sti.nasa.gov
- Fax your question to the NASA Access Help Desk at (301) 621-0134
- Telephone the NASA Access Help Desk at (301) 621-0390
- Write to:
  NASA Access Help Desk
  NASA Center for AeroSpace Information
  7121 Standard Drive
  Hanover, MD 21076–1320

NASA/TP—1999–208640

The SERTS–97 Rocket Experiment to Study Activity on the Sun: Flight 36.167–GS on 1997 November 18

Marvin Swartz, Charles E. Condor, Joseph M. Davila, J. Patrick Haas, Stuart D. Jordan, David L. Linard, Joseph J. Miko, I.Carol Nash, Joseph Novello, Leslie J. Payne, Thomas B. Plummer, Roger J. Thomas, and Larry A. White
NASA Goddard Space Flight Center, Laboratory for Astronomy and Solar Physics
Greenbelt, Maryland

Jeffrey W. Brosius
Raytheon STX Corporation
Lanham, Maryland

William T. Thompson
Space Applications Corporation
Largo, Maryland

National Aeronautics and
Space Administration

Goddard Space Flight Center
Greenbelt, Maryland 20771

February 1999

Available from:

NASA Center for AeroSpace Information
7121 Standard Drive
Hanover, MD 21076–1320
Price Code: A17

National Technical Information Service
5285 Port Royal Road
Springfield, VA 22161
Price Code: A10

Goddard Space Flight Center
SERTS EXPERIMENT PERSONNEL

Principal Investigator: Joseph M. Davila
Heads all phases of the SERTS Program. Design, Assembly, Test, (DAT) Analysis, Planning

Co-Investigators: Jeffrey W. Brosius, Stuart D. Jordan, Roger J. Thomas, and William T. Thompson
Science Planning, Data Analysis, DAT.

Experiment Personnel: Charles E. Condor, David L. Linard, and Marvin Swartz
Design, Align, Test, Calibration of Experiment, Detector, Vacuum systems, CCD cooling, DAT.

Electronics Personnel: J. Patrick Haas, Joseph J. Miko, Joseph Novello, and Leslie J. Payne
CCD & Detector operation, computer programming, control systems, data readout & control, DAT.

Experiment Mechanical Designer: Larry A. White

Electronic Fabrication Personnel: I. Carol Nash and Thomas B. Plummer

Multilayer Coatings and Optics Personnel: Ritva A.M. Keski-Kuha

Stuart Jordan, Jeffrey Brosius and William Thompson are solar physicists working on analysis of the SERTS data and solar theory. Joe Novello designed the Ground Support Equipment and cabling; Carol Nash and Thomas Plummer built the electronic circuits, cables and boards; Larry White designed the detector mechanical structures; Ritva A.M. Keski-Kuha was responsible for the vacuum deposition of the multilayer coatings on the grating. ALL of the other SERTS experiment personnel, although listed in their specialties, participate in many different phases of design, assembly and testing at Goddard Space Flight Center(GSFC) and White Sands Missile Range, and in assembling and operating the computer controlled experiments during its calibration runs at GSFC and/or Rutherford Appleton Laboratory in England.

Werner M. Neupert, the original principal investigator, and Gabriel L. Epstein, former Co-Investigator, were part of the team that designed and built the original SERTS rocket payload. The success of the early flights proved that SERTS was an excellent instrument for solar studies and provided the foundation upon which advancements in detector, grating, and telescope design could be incorporated for future flights.

Members of the GSFC Optics Branch who were responsible for the vacuum deposition of the multilayer coatings on the gratings, or were involved in the alignment of the telescope and spectrograph optics, are Ritva A.M. Keski-Kuha, Jeffery S. Gum, Geraldine A. Wright, and Charles M. Fleetwood Jr.

Michael J. Amato designed the mechanical interface between the SERTS experiment and the calibration drive mechanism which was mounted inside the vacuum chamber at Rutherford Appleton Laboratory (RAL).

Barry Kent was responsible in the UK for the assembly and operation of the RAL vacuum chamber with the SERTS x-y adjustment mechanism for alignment and the cooling system for the CCD. The EUV Calibrated Source was provided by J. Hollandt and B. Wende from the Physikalisch-Technische Bundesanstalt in Germany.

ASSOCIATED SCIENTISTS

The SERTS team also consists of a group of international Associated Scientists with whom we routinely collaborate. These individuals have been actively involved in supporting the calibration, analysis, and interpretation of SERTS data for a number of years.

Name	Institution	Principal Interest
William Behring	Goddard Space Flight Center, USA	Line Identification
Anand Bhatia	Goddard Space Flight Center, USA	Atomic Physics
Richard Harrison	Rutherford Appleton Laboratory, UK	Calibration
Francis Keenan	University of Belfast, UK	Atomic Physics
Massimo Landini	University of Florence, Italy	Atomic Physics
Helen Mason	Cambridge University, UK	Atomic Physics
Peter Young	Cambridge University, UK	Atomic Physics

SERTS Sounding Rocket World Wide Web site:

We also maintain a SERTS WWW site. At this site, one can obtain pictures of integration, launch and recovery, spectroscopic line lists, lists of recent publications, and information on upcoming launches.

Visit the SERTS Home Page on the World Wide Web at:

HTTP://ORPHEUS.NASCOM.NASA.GOV/SERTS

EXECUTIVE SUMMARY

This paper describes mainly the 1997 version of the Solar EUV Rocket Telescope and Spectrograph (SERTS–97), a scientific experiment that operated on NASA's suborbital rocket flight 36.167–GS. Its function was to study activity on the Sun and to provide a cross calibration for the CDS instrument on the SOHO satellite. The experiment was designed, built, and tested by the Solar Physics Branch of the Laboratory for Astronomy and Solar Physics at the Goddard Space Flight Center (GSFC). Other essential sections of the rocket were built under the management of the Sounding Rockets Program Office. These sections include the electronics, timers, IGN despin, the SPARCS pointing controls, the S–19 flight course correction section, the rocket motors, the telemetry, ORSA, and OGIVE. Documents describing these sections and their operation can be acquired by contacting Frank Lau, Payload Manager, Code 810, at NASA/GSFC, Wallops Flight Facility, Wallops Island, Virginia 23337. There were many people at White Sands Missile Range and Wallops Flight Facility who worked on the payload and rocket sections listed above; they all were instrumental in the success of the flight. Their names are listed in the Appendix.

The SERTS–97 Rocket Experiment to Study Activity on the Sun

Table of Contents

I. INTRODUCTION

Ultraviolet observations of the Sun were made from space as early as 1946 using rocket experiments that reached altitudes above most of the earth's atmosphere. A series of Orbiting Solar Observatories was launched in the 1960s and early 1970s to observe the Sun from ultraviolet through the gamma-ray region of the spectrum. At the end of this period, a sophisticated group of instruments on the Skylab Apollo Telescope Mount provided remarkable images of the Sun from the visible through the X-ray region. Such surveys made it clear that the extreme ultraviolet (EUV) spectral band, ~100 – 1000 Å, offers an extraordinarily rich source of detailed information about physical conditions in the important outer layers of the Sun's atmosphere, the upper transition region and corona. But solar EUV images at that time either confused spatial and spectral measurements by overlapping or else had very modest resolutions. In order to overcome these limitations, Neupert, Epstein and Thomas at GSFC developed an imaging spectrometer with the following components: (1) a telescope that forms a real image of the sun in visible and EUV wavelengths onto the spectrograph entrance aperture; (2) a novel aperture with a narrow slit section for spectral line measurements and two wider openings to produce spectroheliograms; (3) a stigmatic grating with high spatial and spectral resolutions; and (4) a film camera to record the data over a large EUV waveband. Thus the Solar EUV Rocket Telescope and Spectrograph (SERTS) instrument was born. Many scientific papers were and are being published from the data recorded on numerous flights in the late 1980s and early 1990s with this instrument. SERTS has continued to evolve into an instrument with a multilayer coating on its grating, and an intensified Charge Coupled Device (CCD) detector replacing the film camera. This new detector and the more efficient multilayer coating have given the instrument much better time resolution and larger dynamic range.

The main objective of the SERTS-97 flight (NASA designation 36.167-GS) on 1997 November 18 was to cross calibrate the SOHO CDS and EIT instruments by observing the same active region on the Sun. For this purpose, the complete SERTS instrument was calibrated at the Rutherford-Appleton Lab in England using the same EUV source that provided the CDS pre-flight calibration, a source which itself had been calibrated at the BESSY synchrotron in Germany. The flight also carried an EUV full-sun monitor from the University of Southern California; its data will help to calibrate measurements taken by the SOHO/CELIAS instrument, as well as to validate the model of EUV transmission through the Earth's atmosphere necessary to correct all the primary SERTS measurements. Other objectives of the flight were to extend our study of solar activity to the present rising phase of the solar cycle, and to obtain the data with an improved spectrograph entrance aperture and a higher resolution intensified CCD detector. In addition, we tested an improved set of electronics and data compression system on this flight.

This latest version of SERTS is designed to record spatially resolved images at various discrete wavelengths from highly ionized material in the solar corona in the wavelength range between 298 Å and 354 Å. The design also allows one to record simultaneously with high spectral resolution many narrow spectral lines to accurately determine their wavelength. This is accomplished by a telescope-spectrograph with an intensified CCD imaging detector as the recording and readout device. The telescope focuses a 2-cm diameter image of the Sun onto the entrance aperture of the spectrograph. Light from parts of the solar disk selected by the entrance aperture passes onto the grating, which then forms spectrally dispersed EUV images of those features onto its focal plane, where the imaging detector is placed to record the data. The entrance aperture itself is in the form of an open dumbbell or hourglass configuration. The central narrow-slit section is 3.7 mm long (6.0 arcmin on the Sun) by 21.5 μm wide. This width corresponds to 2 arcsec spatially and .05 Å spectrally. Above and below the central slit are two slots or lobes each 5.3 mm long (8.6 arcmin on the Sun) by 1.8 mm wide (3.0 arcmin). The wider lobes produce spectral images from the few, well isolated, bright emission lines in our bandpass (spectroheliograms), while the central narrow part provides high-resolution spectra of all observable lines along the one spatial dimension of the slit.

The wavelength range 298 Å to 354 Å contains many highly ionized strong lines of several different elements. Some of these lines are from ions of He II, Fe X-XVI, Ni XVIII and Si VIII-XI. Weak lines of the ions Mg V and Mg VI are also observed. The stronger lines tend to be generated over a plasma temperature range of 1.0-2.3 x 10^6 K in the solar corona, while certain weak magnesium lines indicate temperatures of 3 x 10^5 K in the Sun's transition region. The He II line at 304 Å is formed in the lowest part of the transition region at temperatures of 5-10 x 10^4 K, or slightly higher.

The fastest temporal variations in the spectroheliograms are explored by observing a series of images taken about every 5 seconds, which allows for 1-second exposures (data capture) and 4 seconds to readout the CCD image into telemetry. To make more efficient use of the available observing time, however, exposures are usually set to between 3 and 30 seconds or even longer, made possible by the detector's large dynamic range and active cooling.

The use of the narrow slit over any solar feature permits a study of the bulk inflow or outflow of plasma material by the presence of Doppler-shifts toward the red or the blue. Broadening of the spectral line, on the other hand, yields information on flows that take place on spatial scales smaller than the imaging resolution of the instrument.

Certain diagnostic line pairs, such as Fe XII 338.3/352.1 Å, permit the determination of densities at their characteristic temperature of formation. Other pairs of lines that are only slightly affected by density can be used to measure the temperature of the emitting plasma; such a pair is Fe XIV 334 Å and Fe XVI 335 Å. Well before each SERTS flight, the spectral bandpass, exposure sequence, pointing pattern, and integration times are worked out to optimize the type of scientific investigation to be performed during that shot. Final target selection is made the morning of the flight, depending on the Sun's activity at the time. Offset pointing to change targets remains an option that can be carried out at any time during the flight based on real-time developments.

The wavelengths of the EUV emission lines that were observed and identified from the SERTS-97 flight are listed in Table 1. The integrated detector response and "parent" ion for each line are also listed. This list is preliminary, and in particular does not yet include the various calibration factors needed to convert the detector responses into absolute intensity units.

Table 1
Identified Spectral Lines from SERTS-97

λ(Å)	Ion	Integrated Detector Response	λ(Å)	Ion	Integrated Detector Response
303.32	Si XI	285.0	338.28	Fe XII	33.7
303.78	He II	4778.0	339.00	Mg VIII	23.1
304.87	Mn XIV, Fe XV	18.3	340.96	Unknown	7.5
305.80	Cr XII	9.1	341.13	Fe XI	28.4
313.73	Mg VIII	21.1	341.29	Unknown	6.3
314.34	Si VIII	6.0	341.97	Si IX	23.5
315.02	Mg VIII	53.1	342.16	Unknown	5.6
316.14	Unknown	"	342.41	Ca VII	6.9
316.21	Si VIII	52.4	344.96	Si IX	15.4
316.50	Ni XIV	4.2	345.14	Si IX	50.6
317.01	Mg VIII	11.5	345.74	Fe X	39.2
318.11	Fe XIII	26.7	346.85	Fe XII	45.4
319.84	Si VIII	44.5	347.40	Si X	121.8
320.56	Ni XVIII	33.4	348.19	Fe XIII	97.2
320.80	Fe XIII	52.0	349.03	Fe XI	9.1
326.34	Unknown	8.2	349.16	Mg VI	34.3
327.03	Fe XV	37.8	349.87	Si IX	72.1
328.26	Cr XIII	36.2	352.12	Fe XII	86.3
332.78	Al X	76.6	352.68	Fe XI	70.2
334.17	Fe XIV	387.5	353.09	Mg V	9.1
335.40	Fe XVI	3615.0	353.32	Mg V	3.2
			353.81	Fe XIV	85.7

II. DESCRIPTION OF THE INSTRUMENT

The SERTS scientific instrument consists of 6 distinct sections (Figure 1), with each section forming a functional part of experiment. Figure 2 shows the mechanical layout of all the sections assembled as the flight instrument.

Section (1): The forward telescope section with the coarse and fine pointing location sensors aligned with the telescope front face.

Section (2): The spectrograph entrance aperture with its hourglass or dumbbell shaped opening in a disk located at the focus of the telescope.

Section (3): The toroidal grating, 1150 mm away from the aperture disk plane and along the telescope axis.

Section (4): The microchannel-plate CCD detector on the focal plane of the grating; an a1uminum filter; and the camera-head electronics mounted just behind the CCD. (Figure 4 shows the vac ion pumps, valves, and housing not indicated in Figure 1.)

Section (5): The flight-control electronics with interfaces to the camera head, GSE and telemetry.

Section (6): The Hα camera, which receives the reflected image of the Sun from the front face of the entrance-aperture disk, sends the image through its Hα filter, and focuses the Hα image through a doublet lens onto a CCD.

The central bulkhead is the main structure upon which is mounted the entrance-aperture disk (Section 2), the detector (Section 4), and cooling block to provide a heat sink to cool the detector CCD (see Figure 2). Cylinders are attached to both sides of the bulkhead. The forward cylinder holds the telescope and Hα camera with its oven-filter and lens. The rear cylinder, constructed of epoxy-graphite which has a low coefficient of expansion, holds the toroidal grating which focuses the image of the entrance aperture onto its focal plane. The front face of the intensified CCD detector is positioned on the focal plane by using the central bulkhead as its rigid mounting structure. The two outer skins are O-ring mounted to the central bulkhead and also make vacuum tight fits to the door and electronics mounting plate. The experiment is pumped down to 10^{-4} torr or better just before launch. For mechanical layout, refer again to Figure 2. Sixty-four seconds after launch (T + 64 s), the experiment shutter door is opened. At T + 101 s, the pressure outside the rocket is 3.8×10^{-6} torr. The experiment begins its observing sequence at this time; the rocket is then at an altitude of 104 miles (550,000 feet). The pressure inside the experiment is in the neighborhood of 10^{-4} torr and continues to decrease as long as the main experiment door (shutter) is open. See Section 4, for a discussion about operating an open detector in this environment.

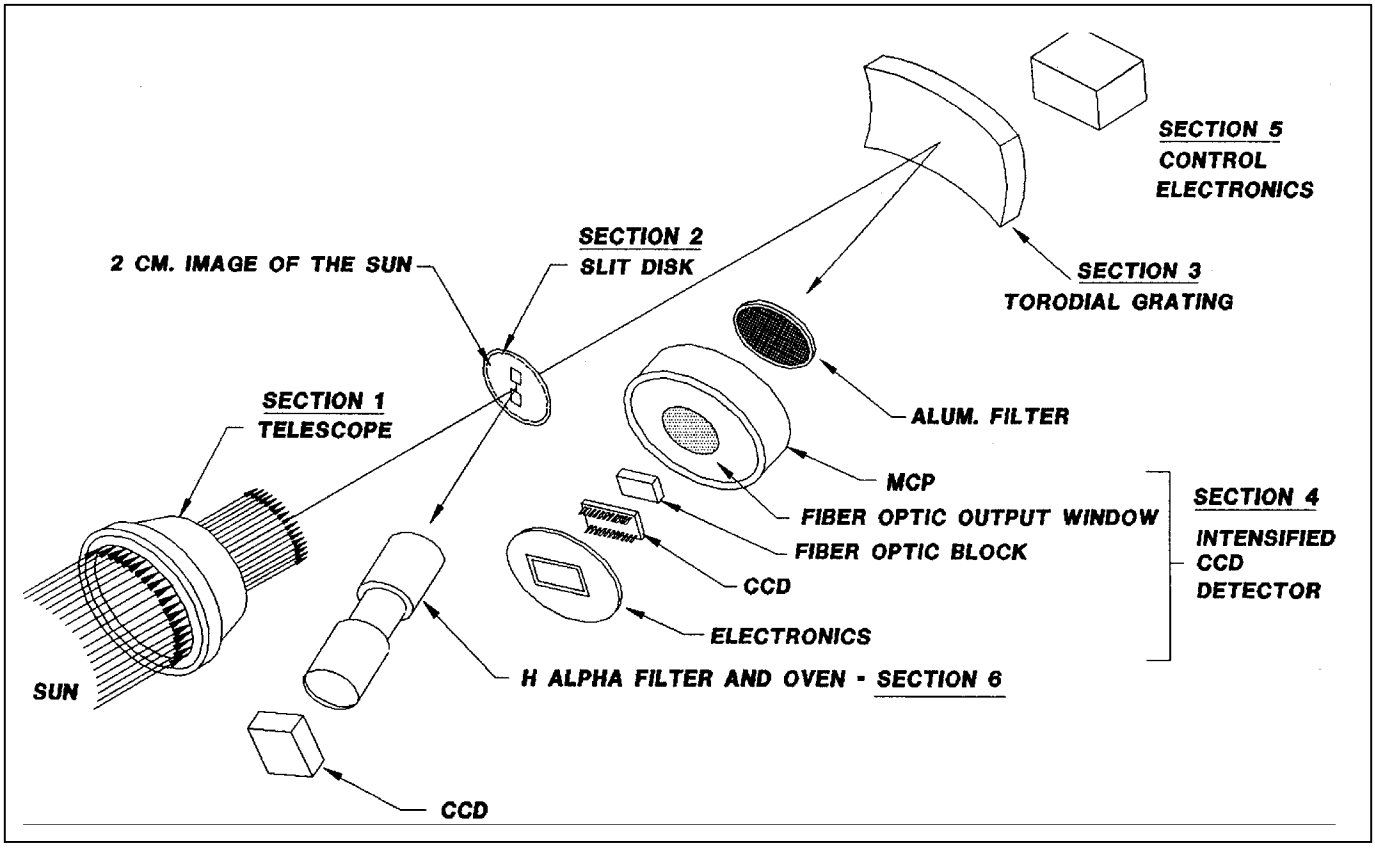

Figure 1. Experiment's major components.

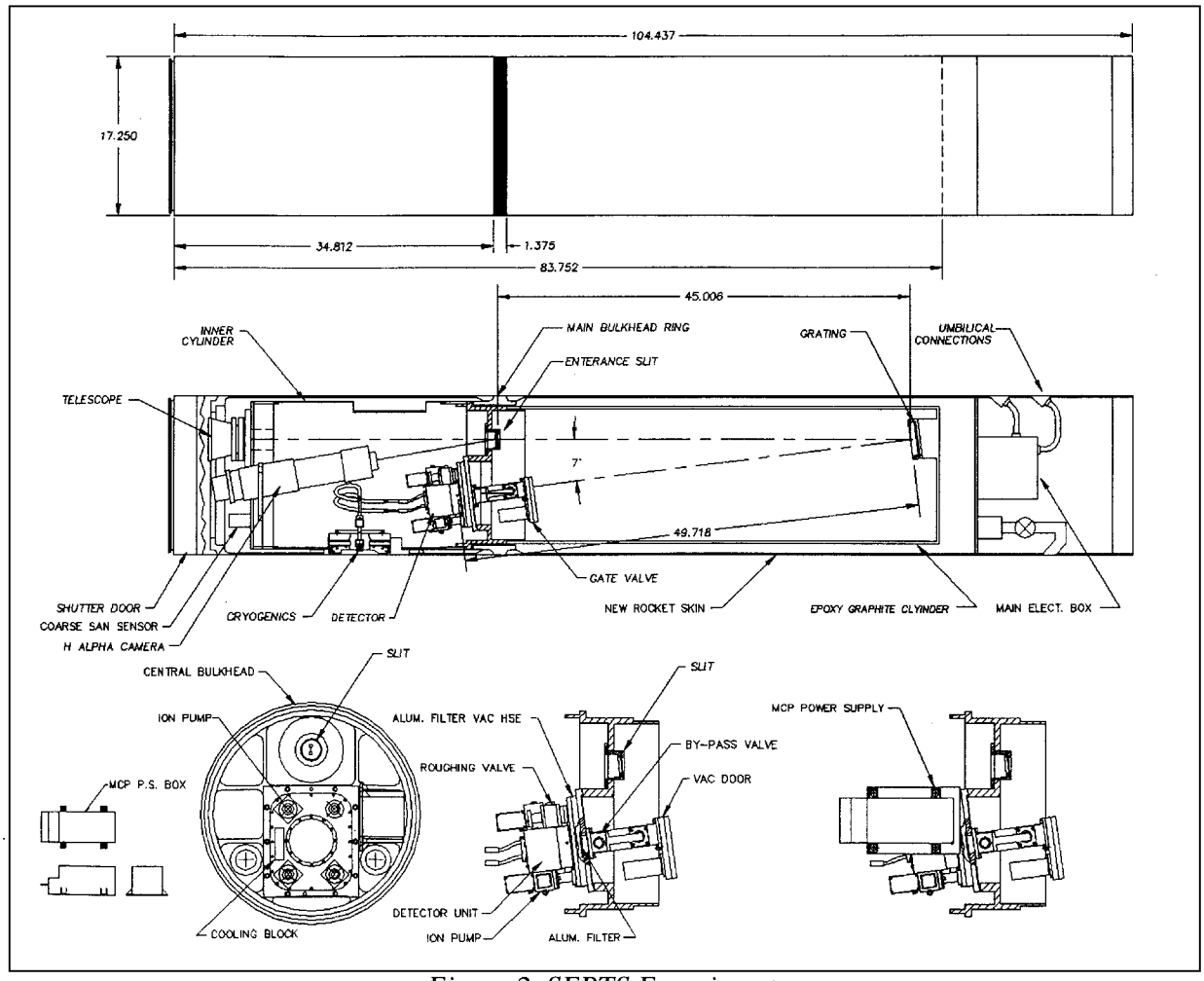

Figure 2. SERTS Experiment.

Section 1: Telescope

The telescope is a grazing incidence Wolter Type II made with a parabolic primary mirror and hyperbolic secondary mirror to extend its focus to the entrance aperture of the spectrometer. The telescope parameters are listed in Table 2. See Figure 2a for telescope assembly drawing.

Table 2. Grazing Incidence Telescope Parameters

Effective focal length	212 cm
Outer F-Number	f/22
Resolution at 304Å	5 arcsec
Geometric Aperture	22 cm^2
Overall Length to focus	80 cm
Size of solar image at slit (full disk)	2.0 cm

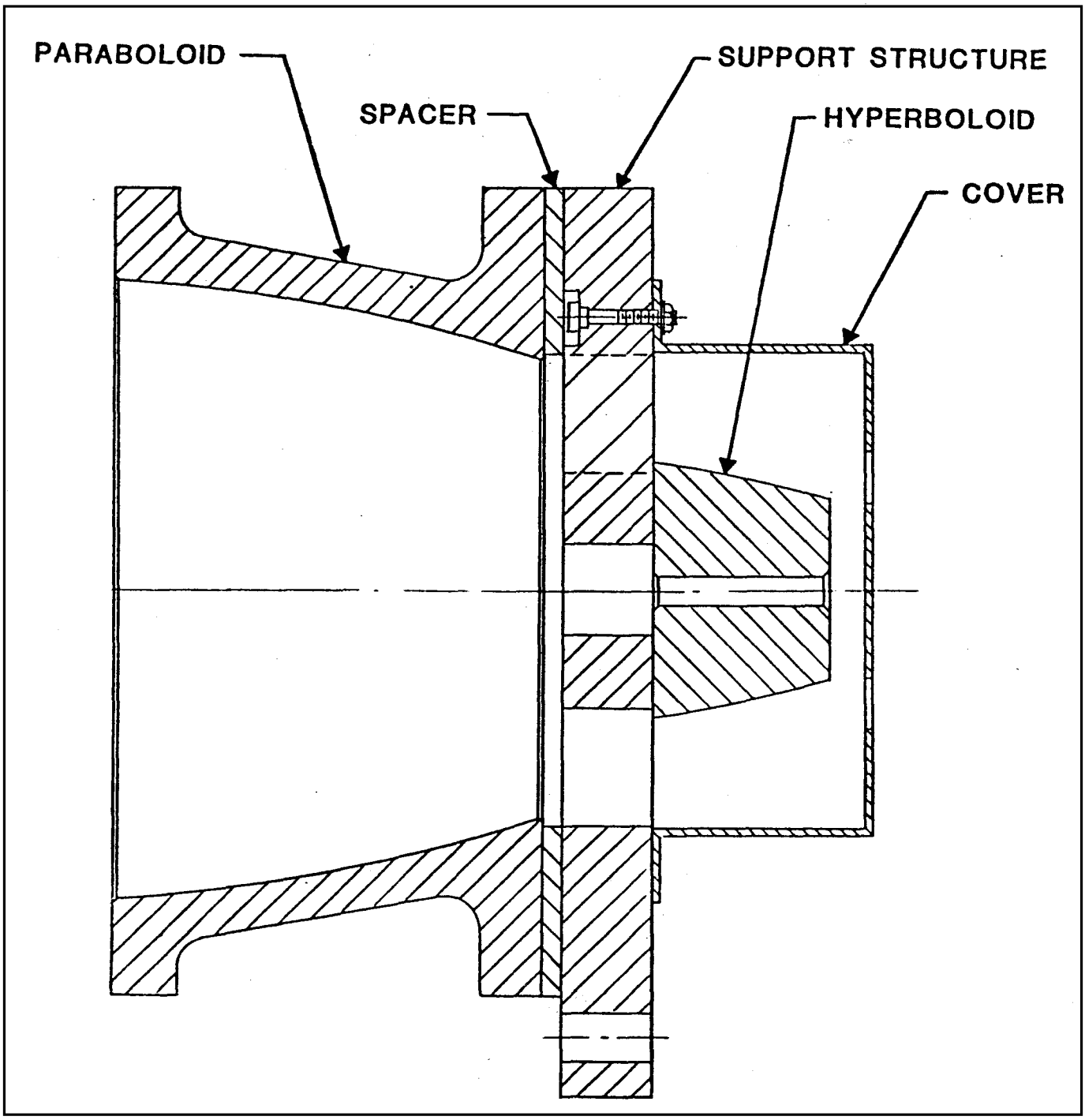

Figure 2a. Wolter Type II Telescope.

FIGURE 3

DISK WITH ENTRANCE APERTURE

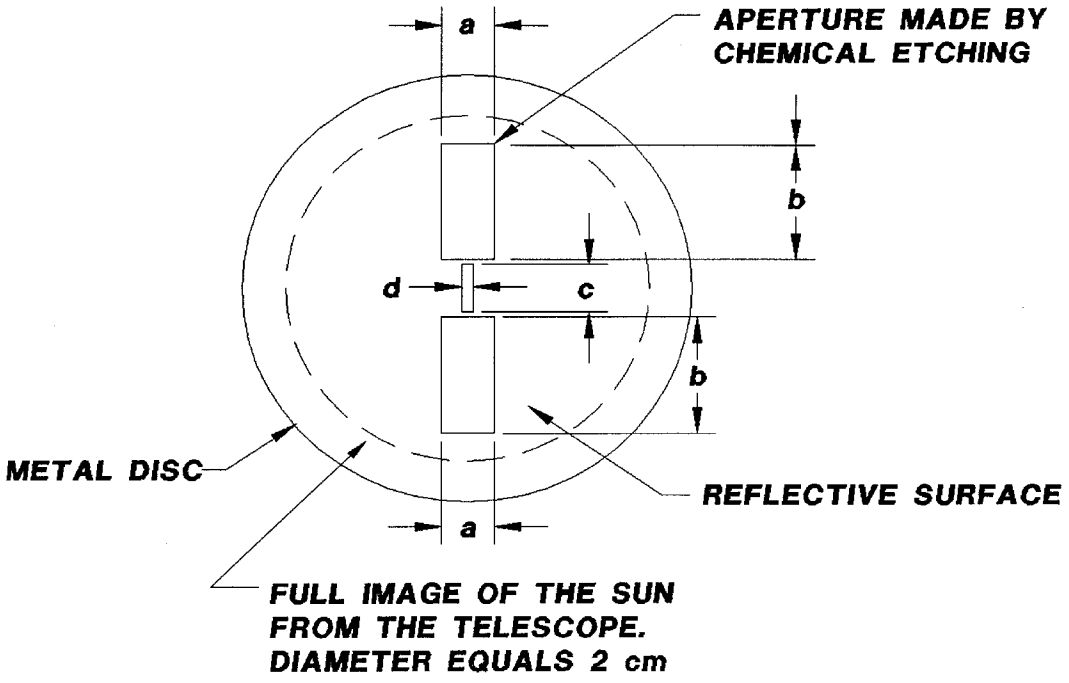

TABLE 3

APERTURE-SUN DIMENSIONS

APERTURE DIMENSION	SUN VIEW	SUN DIMENSION
a. 1.850 mm	3.0 arc min	82,000 miles
b. 5.275 mm	8.6 arc min	230,000 miles
c. 3.7 mm	6.0 arc min	160,000 miles
d. 21.5 microns	2.1 arc sec	950 miles

The primary and secondary mirrors are both made of low expansion Zerodur glass and are held in alignment by a spider structure also made of Zerodur.

Section 2: Entrance Aperture

The spectrograph entrance aperture (also referred to as the entrance slit or just slit) is used to select the specific region of the Sun to be analyzed. It is centered on the telescope axis at a position just slightly inside the telescope's Gaussian focus. The slit-dumbbell configuration is shown in Figure 3; the aperature dimensions are given in Table 3 along with the corresponding coverage on the Sun. Table 3 is on the same page as Figure 3 for clarity, since both are interrelated.

Section 3: Grating

The grating is a glass piece formed into a rectangular block with the reflecting surface made into a torodial configuration with 2 radii of curvature, which are highly polished. This toroidal surface has a gold layer upon which the ruling is formed. The ruling density is 3600 lines/mm with a blaze of 3.1°, a magnification 1.1 on the focal plane and a spectral dispersion of 2.2Å/mm. A multilayer coating of indium and silicon is deposited on the grating with spacing chosen to optimize the wavelength range between 280Å – 360Å. The multilayer coating enhances the reflectance across this range by a factor of up to 8, which allows us to operate our detector with an integration time ≥ 1 second. The detector is mounted on the focal plane of the grating to cover the wavelength range between 298 Å and 354 Å. The grating parameters are given in Table 4.

Table 4. SERTS-97 Spectrograph Grating Parameters

ITEM	VALUE
Ruling density	3600 lines/mm
Spatial magnification	1.1
Radius of curvature	
Sagittal	1200.02 mm
Tangential	1209.67 mm
Measured surface accuracy	≤0.08 λ ptp @ 6328 Å
Blaze angle (design)	3.1 deg
Spectral Range (1st order)	298 – 354 Å
Radius of cylindrical focal plane	647.2 mm
Spatial plate scale	11.3 μm/arcsec
Dispersion at focal plane	2.2 Å/mm

Section 4: The Intensified CCD Detector

Refer to Figures 4, 5 and 6. EUV images from the grating are focused onto the microchannel-plate front surface where the incident photons are converted to electrons with a photoelectric efficiency of about 20%. When an electron is produced in a channel, a voltage across that microchannel causes each electron to be multiplied, as each channel then acts as a microscopic electron multiplier. As a packet of electrons emerges at the output end of the channel, they are accelerated by 5000 Volts across a .5 mm gap and then through 1000 Å of Al into a P-20 phosphor deposited on a fiber optic window. The high-energy electrons are converted by the phosphor into 5500 Å photons with a gain of approximately 20 photon/electron. These photons then pass through the fiber optic window made with 6-μm fibers. A fiber optic transfer block with 4-μm fibers couples the image from the output window into a CCD which is bonded to the same transfer block. The total gain of the MCP tube depends on the MCP voltage and could approach 40,000 overall if needed. However, the gain must be set so that any single detected photon at the MCP will yield enough electrons stored in a CCD pixel to overcome the noise. The MCP on our 1997 flight was set at 700 Volts which gives it an electron gain of about 90 (total gain of 1800). For gain vs. voltage, see reference by Dominic J. Ruggieri. A diagram of the MCP tube may clarify how a MCP operates (see Figure 5 [our modified drawings from Ruggieri]). Table 5 is a summary of the detector characteristics. The resolution of the detector on SERTS-97 was 30 lp/mm. An improved detector is under development with a resolution of 40–45 lp/mm, corresponding to a pixel size of 11.0–12.5 μm.

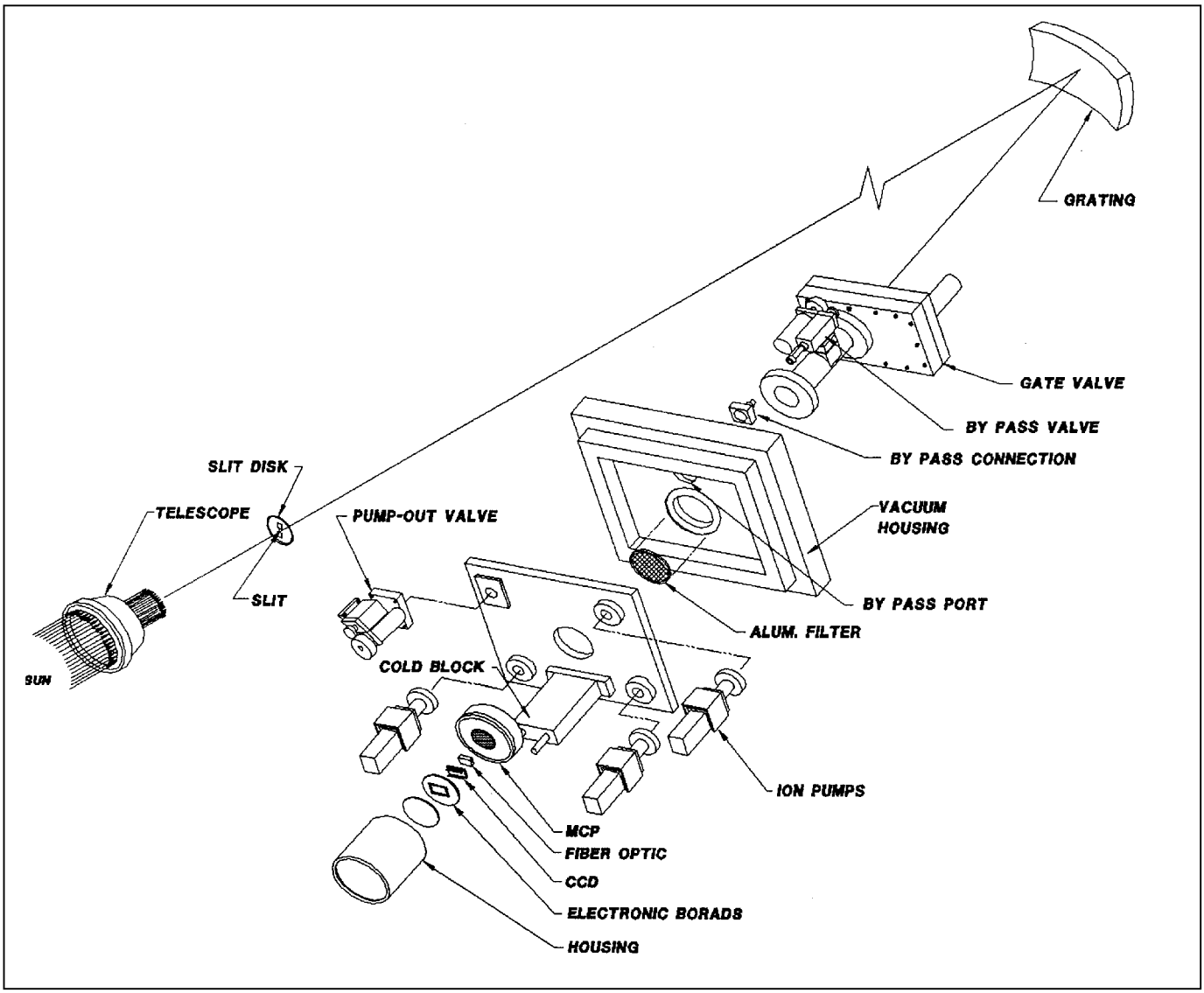

Figure 4. SERTS Detector Opto-Mechanical Layout.

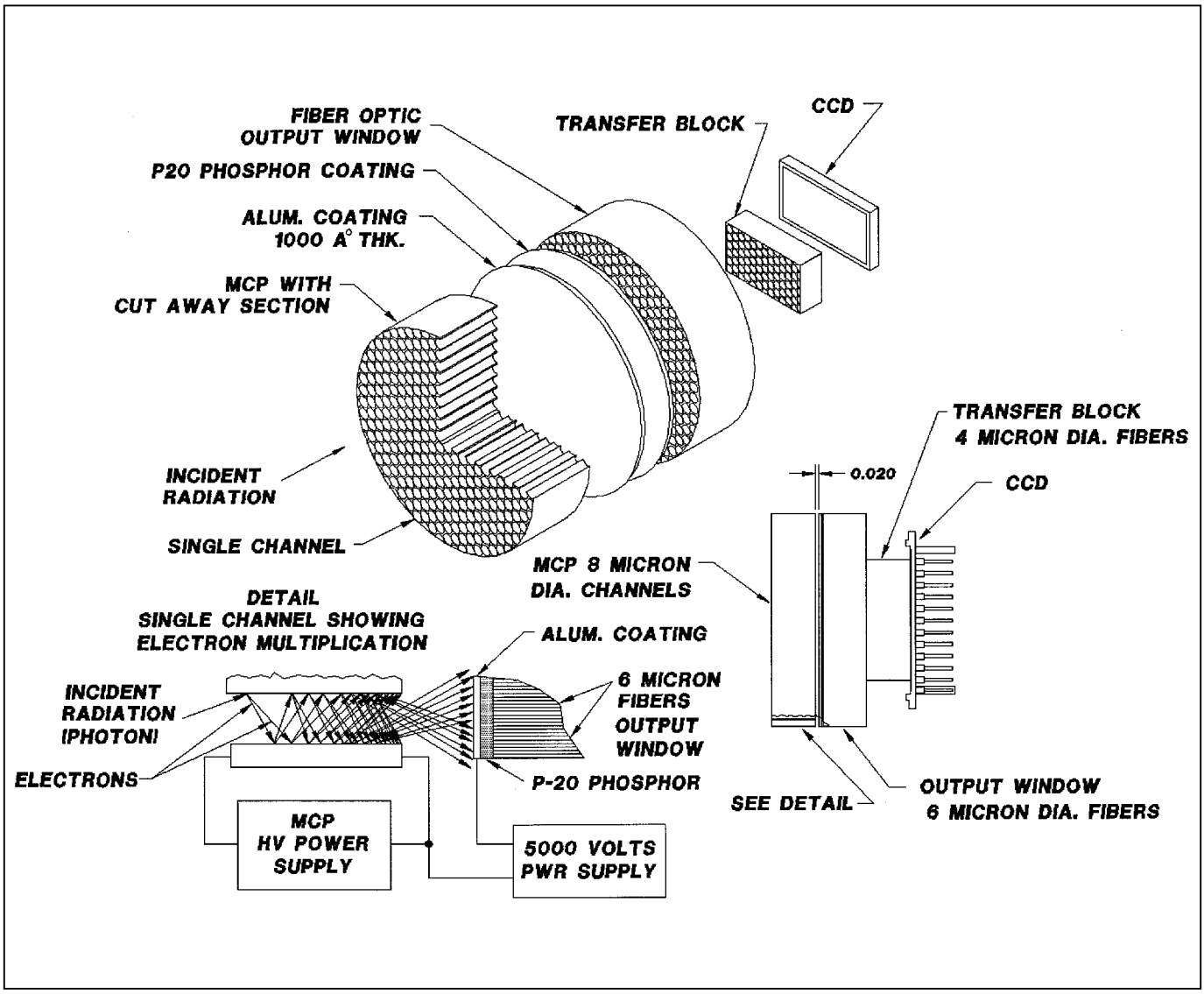

Figure 5. MCP Detector Camera Head.

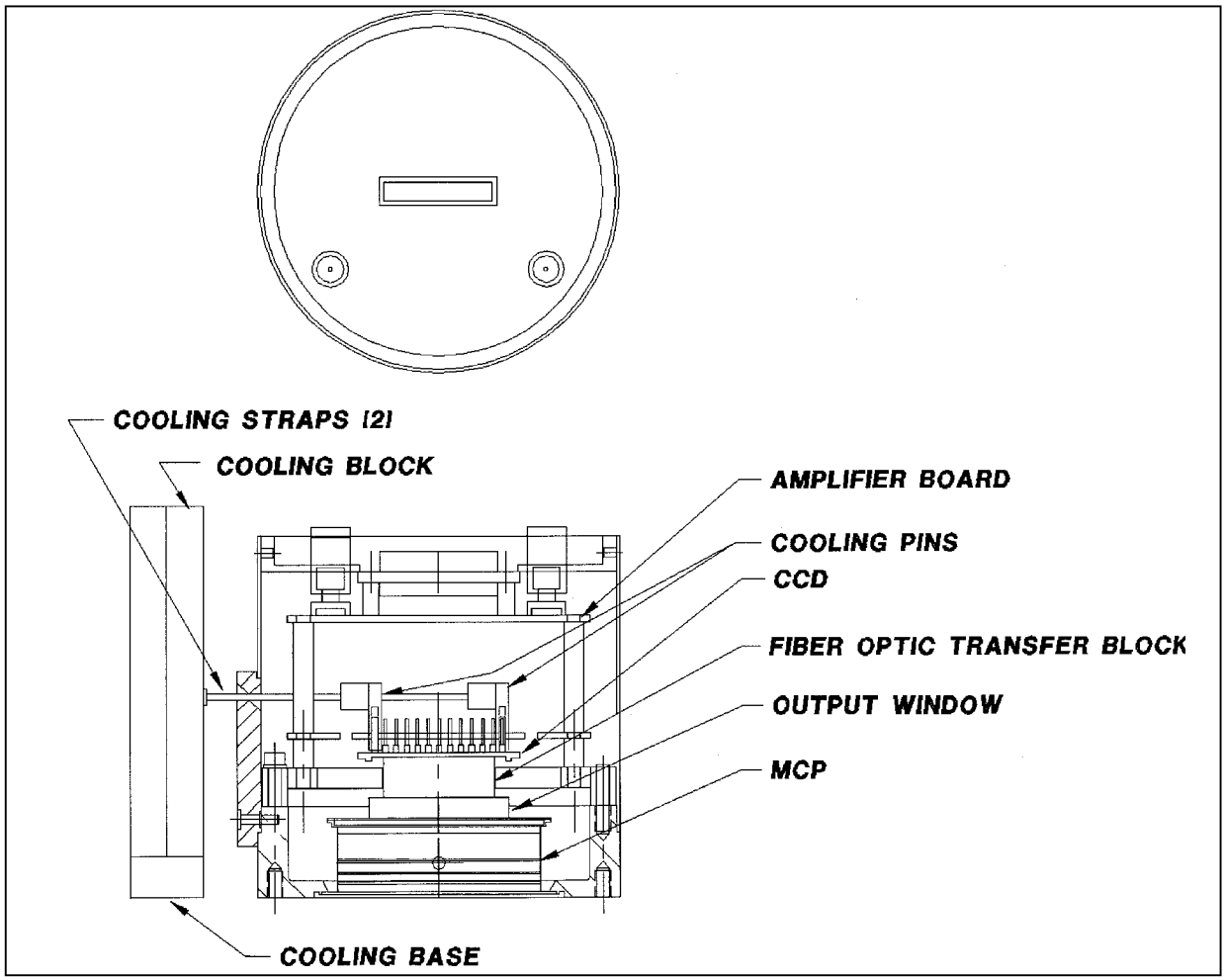

Figure 6. Assembled MCP and CCD.

Table 5. Summary of Detector Characteristics

MCP outer diameter	25mm
MCP channel diameter	8 μm
Quantum efficiency of MCP at 300 – 350 Å	20%
Fiber-optic output window	6-μm fibers
Fiber-optic coupling block	4-μm fibers
CCD pixel size	9 μm
CCD array	3072 x 2048
Phosphor conversion gain	20 photon/electron
CCD readout rate	1.2 x 10^6 pixel/s
Readout noise	20 electron
CCD electrons per single detected event	25 electron (design)
A/D converter	12 bit
Dynamic range	4095 (design)
Aluminum filter transmission	40% at 304 Å
Data compression factor	1.7
Detector resolution	30 lp/mm at 2537 Å
MCP tube input window	none

The absence of an input window presents certain unique challenges during a rocket flight, which influence the design of the detector. The vacuum should be at 10^{-6} torr in the detector during its operation to ensure that no arcing will occur when the microchannel plate voltage and the phosphor high voltage are enabled. A vacuum tight door and housing provide the vacuum enclosure. Vac ion pumps must be operating continuously, except during the CCD integration mode in the observing sequences, to keep the vacuum in the 10^{-6} torr range. See Figure 4 for the vacuum system layout and its components. When the detector door is opened 94 seconds after launch, the pressure in the experiment is ≤ 1 μm. There is a thin Al filter to separate the experiment pressure from the detector pressure. The by-pass valve around the filter is closed before the detector door is opened; at all other times, the by-pass valve will be open to prevent a build up of pressure across the Al filter.

The cooling system for the CCD is a block of copper that is cooled by LN_2 vapor and is connected by copper braid to the CCD pins (See Figure 7). The cooling line goes through the rocket skin into the cooling block, which acts as a heat sink. The cooling line is disconnected from the rocket about 70 minutes before launch. A CCD temperature of –20°C is desired during the data-gathering phase of the flight to reduce the thermal noise in the detector essentially to zero. An improved cooling system is being developed that will be connected through the skin until T - 0 at which time the cooling lines will be pulled away as the rocket is launched.

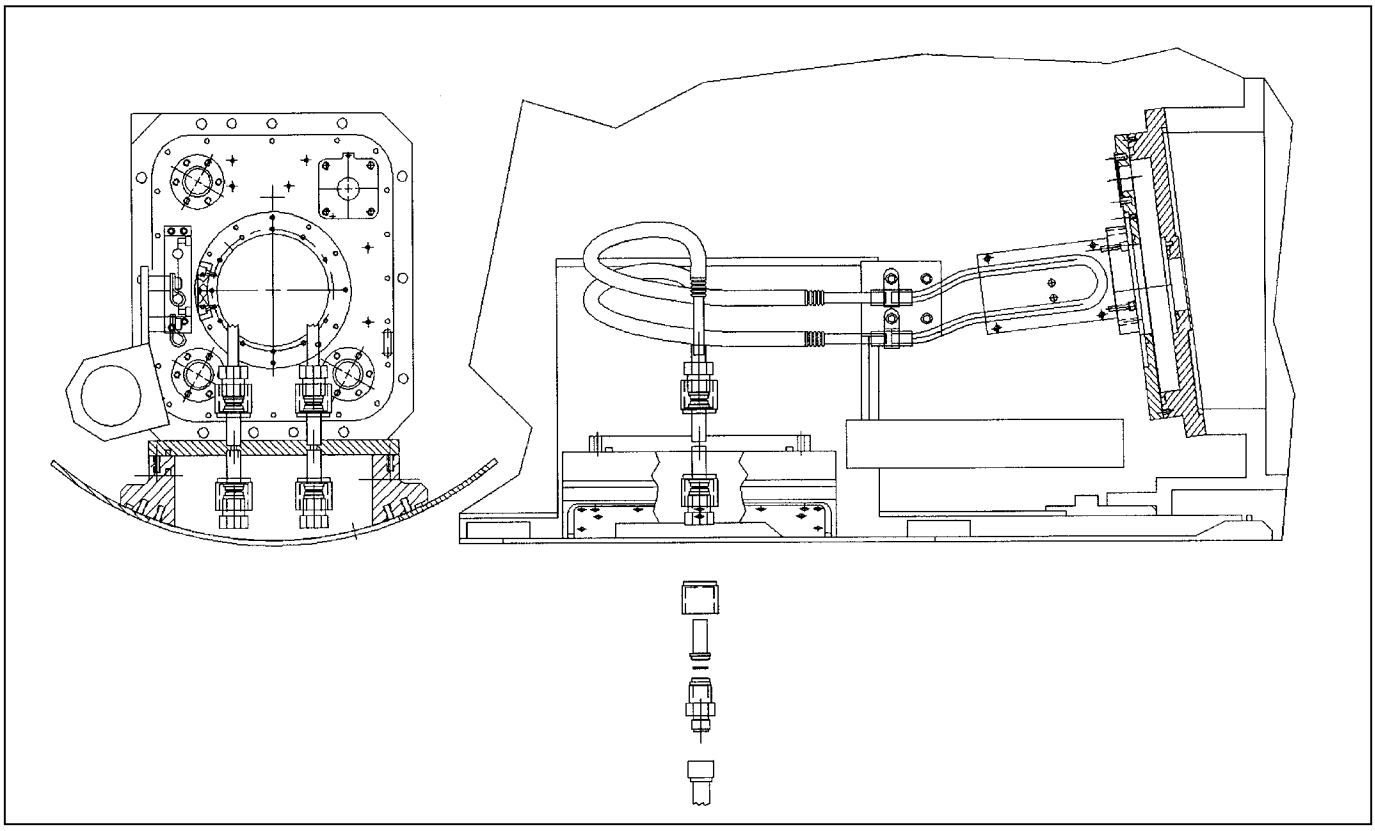

Figure 7. Cooling Block and Tubing.

In order to describe how the detector functions, we present here an equation which follows each detected event through the "gain" of the MCP and finally ends as a number of electrons stored in a pixel in the CCD.

Equation 1

$$(IF)(A_1)(QE_{MCP})(G_1)(T_{1\text{-}AL})(G_2)(T_2)(QE_{ccd})(A_2/R) = \text{electron/pixel}_{ccd}/s$$

Table 5a. Description of Symbols in Equation 1.

Symbol	Description	Units	Value
IF	Input flux	photons/cm^2/s	10^7 (calculated to produce a single event)
A_1	Channel area	cm^2/channel	$50x10^{-8}$
QE_{MCP}	Quantum efficiency of MCP	electron/photon	0.20
G_1	Gain of MCP tube (selected by voltage across MCP)	(none)	90 (MCP=700 V selected for SERTS–97)
T_1(AL)	Electron transmission through Al filter	(none)	0.94
G_2	Phosphor gain	photon/electron	20
T_2	Estimated transmission through the fiber optic	(none)	0.70
QE_{CCD}	Conversion efficiency of CCD at 5500Å	electron/photon	0.40
A_2/R	A=area/CCD pixel R=resolution^2/channel	(9 μm)^2 /pixel (16.5 μm)^2/channel	0.3

A_2/R is the estimated reduction in electrons that fall into a single CCD pixel due to the spread of the electrons from a single MCP channel.

The minimum input flux required that will produce 1 electron/s per MCP channel at its entrance is set by the first three elements of equation 1,

$[\ (IF)(A_1)(QE) = 1\ ] :: (IF)(50x10^{-8}\ cm^2)(0.20\ electrons/photon) = 1\ electron/s$

$IF = 1/10x10^{-8} = 10^7\ photons/cm^2/s$

Substituting the values from Table 5a into Equation 1, and using the input flux of 10^7 photon/cm^2/s, we have:

$(10^7\ photons/cm^2/s)(50x10^{-8}\ cm^2)(.2)(90)\ (.94)(20)(.70)(.4)(9^2/16.5^2) = 142\ electron/pixel_{CCD}$

Theoretically, this should give us a count of 5, well above the noise level of the CCD. If we reduce the gain of the MCP by a factor of 5, then 1 detected event would produce 28 electrons in a CCD pixel. This is close to the design parameters of the electronics.

The strip current provides the electrons to replenish those lost in a channel when a detected event (photon) is converted to an electron and multiplied down the channel. To avoid saturation or gain degradation, the total current to exit at the back of a single MCP channel should not exceed 1/10 of the strip current for that channel. The total strip current in the 25-mm MCP tube we use is approximately 30 μ-amp. The area of the MCP is:

$\pi\ x\ (25/2)^2 = 500\ mm^2$; that of a single channel is: $50x10^{-6}\ mm^2$ or 50 μm^2.

Active area of a tube = 60%, therefore $(500x10^6)(.6) = 300x10^6\ \mu m^2$

$300x10^6\ \mu m^2/50\ \mu m^2 = 6x10^6$ channels in a MCP tube of 1-inch diameter.

30 μ-amp $(.1)/6x10^6$ channel $= 5x10^{-13}$ amp/channel $= 5x10^{-13}$ coulomb/channel/s

electron change = $1.6x10^{-19}$ coulomb/electron

$$\frac{5x10^{-13}\ coulomb/channel/s}{1.6x10^{-19} coulomb/electron} = 3.1x10^6\ electron/channel/s$$

Dividing by the gain of the MCP (700 V = gain of 90), we now have the maximum number of electrons or detected-events per second at the entrance of a channel that the tube can receive and not effect the gain of the MCP.

$$\frac{3.1x10^6\ electron/channel/s}{90} = 3.4x10^4\ detected\text{-}event/channel/s$$

If the gain of the MCP is reduced by a factor of 5, then it could receive $1.7x10^5$ detected-events/channel/s without the gain being affected.

If 10^7 photon/cm^2/s is the input flux to produce 1 detected-event per channel, then $3.4x10^{11}$ photon/cm^2/s is the maximum input flux at the MCP that the tube could receive and remain linear. 10^7 photon/cm^2/s falling on the entrance to the microchannel plate will produce 1 electron/s in each of the channels that are within this flux area. The gain of the phosphor and a gain selected across the MCP tube must be enough to overcome all losses in the other segments of the tube including the Al coating, to store 25 electrons in a CCD pixel. This number is chosen to be greater than the "read out noise" (20 electrons) accumulated in each CCD pixel in 1 s. When this CCD pixel voltage of 250 μV (10 μV per stored electron) is read-out and sent through an amplifier with a gain of 10 to the A/D converter, a count of 1 is registered in the A/D output.

For an integration time of 1 s, then, the controlling factors to determine the number of electrons in a CCD pixel for a count of 1 out of the A/D converter when 10^7 photon/cm^2/s fall on the MCP, are the gain of the MCP, the gain in the phosphor, and the gain of the amplifier following the CCD readout. However, the phosphor voltage is set at 5000 V and the amplifier gain is also set. The MCP voltage is then the only variable factor that can be programmed that will determine the MCP gain to control the number of electrons that will be stored in a CCD pixel for an A/D readout of 1 count.

Full-well capacity (FWC) in the Kodak CCD is 80,000 to 100,000 electrons. Using 100,000 electrons as FWC, and 25 electrons for a count of 1 at the A/D converter, our dynamic range should be 4000. This requires an A/D of 12 bits. This also suggest that the maximum flux falling on the MCP should be no more than 10^7x4000 = $4x10^{10}$ photon/cm^2. This is well below $3.4x10^{11}$ photon/cm^2/s, the saturation point of the MCP. The resolution of the detector is most influenced by the spread of the electrons as they exit from the MCP tube and convert to photons at the phosphor. The output from a MCP channel falling on the CCD will cover more than one CCD pixel. Our measured resolution is 30 lp/mm (corresponding to a 16.5-µm pixel size). If $A_2/R = .3$, then we estimate that only 30% of the electrons from a single MCP channel will fall into a CCD pixel when it aligned with that MCP channel. The 16.5-µm pixel size of the beam falling on the CCD is shown in the diagram in Figure 8. Note, however, that the output from a single MCP channel will add electrons into the adjacent CCD pixels, as well.

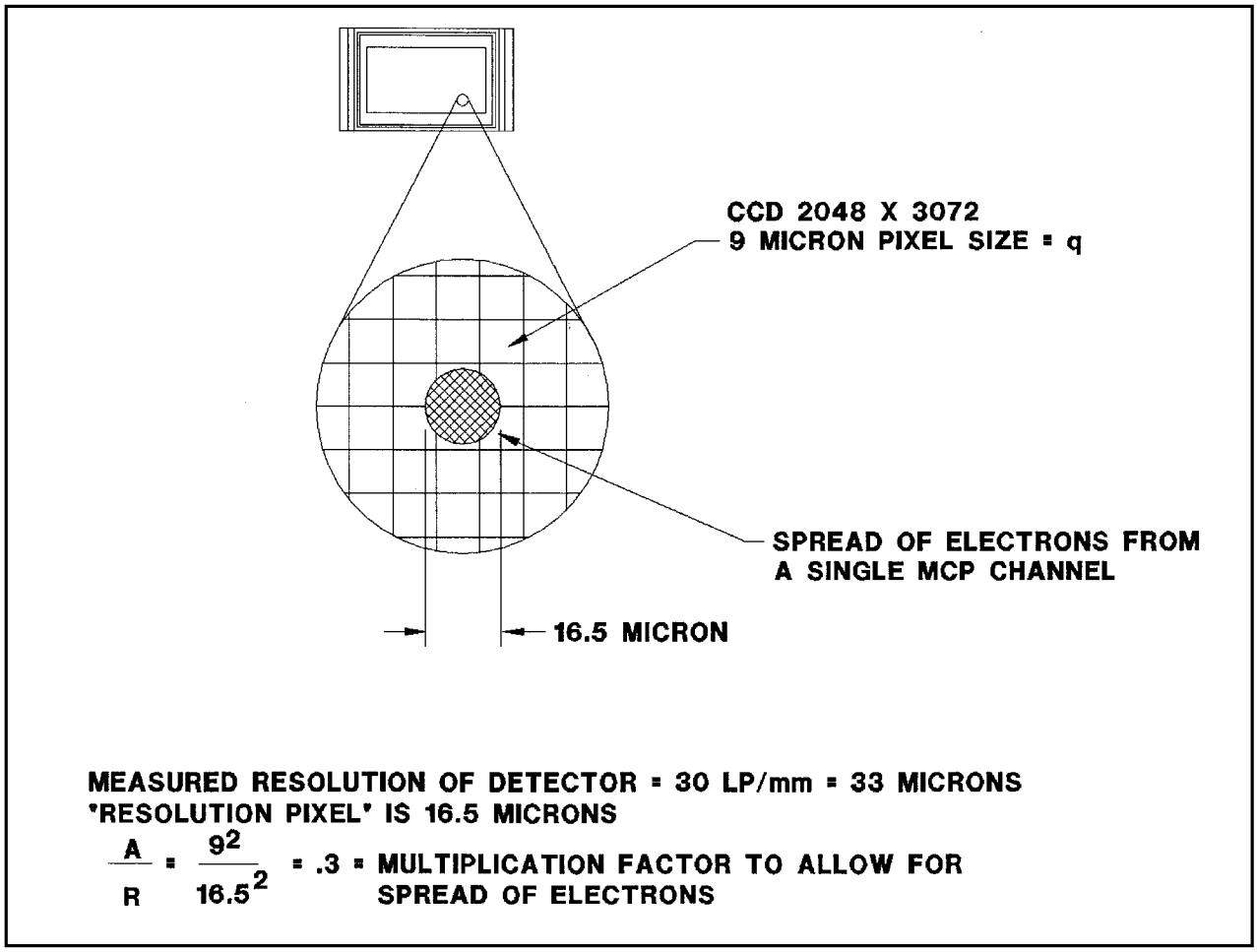

Figure 8. Electrons spread into CCD.

Section 5: Electronics

The camera electronics are composed of an electronics box, main power supply, power amplifier box, a high-voltage power supply for the MCP, and a HV power supply for the vac ion pumps. The computer-based controller (Transputer) in the main electronics box is a programmable unit to generate the observing sequences during the flight and to control the detector when interfaced to the GSE. During flight, each pixel of the image from the CCD is digitized to 12 bits and then compressed by a factor of 1.7 before it is transferred to telemetry. All images are stored at the ground station. A block diagram of the electronics circuits is given in Figure 9.

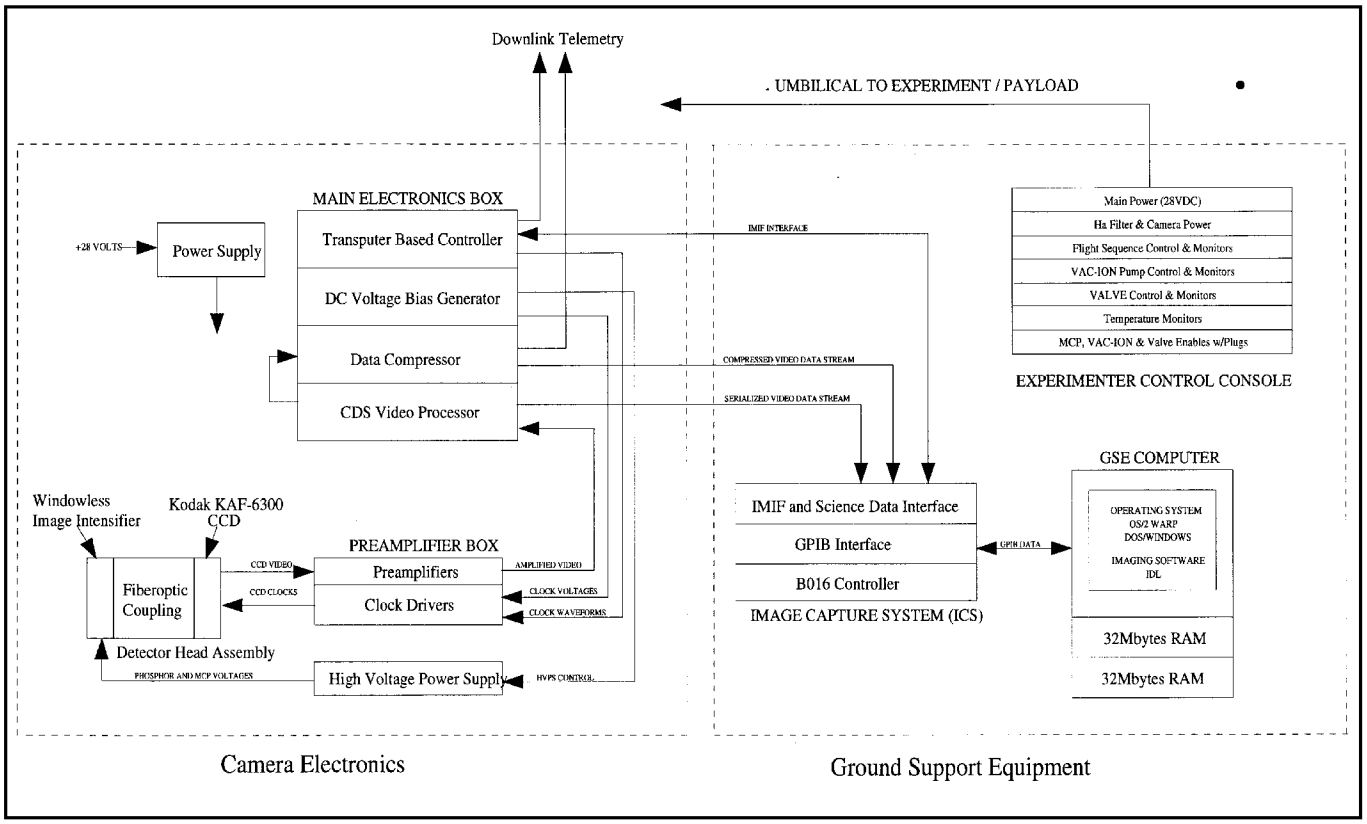

Figure 9. SERTS General Purpose Camera System and GSE.

The ground support system (GSE) receives the images during ground tests by an umbilical cable attached at the rocket skin to a pull-away connector. A second umbilical cable, from the GSE power & control unit to the experiment, allows one to turn on the 28 V to the camera electronics and run the camera with pre-selected parameters. These images are recorded and analyzed during focusing and wavelength calibration in the lab.

The GSE also allows the operator to control: the vac ion pumps, the Hα-camera operation, the MCP high-voltage power and enable, and opening and closing of the gate valve and detector door. Four enabling safety plugs are available, and the correct one must be installed to allow the operator to activate any of the above functions. Also, the GSE provides monitor readouts of various detector temperatures, currents, and voltages.

Section 6: Hα Camera

Light from the Sun's image that does not pass through the spectrograph entrance aperture is reflected toward the Hα camera, which focuses it through an Hα filter onto a solid-state CCD where it is recorded and sent to the ground station via a telemetry video link. This allows us to observe the Hα image in real time on the ground during the rocket flight. The whole reflected image of the Sun from the aperture has the hourglass opening itself superimposed as a black feature at the center of the frame. In this way we can immediately see how the entrance aperture will cover the selected region on the Sun's disk. In-flight corrections can be made by sending commands to move the rocket pointing axes in small steps which causes the telescope to move the solar image across the entrance aperture so that it covers a new area. Refer to Figures 1 and 2 to locate the Hα camera in the experiment, and to Figure10 for a diagram of the Hα camera.

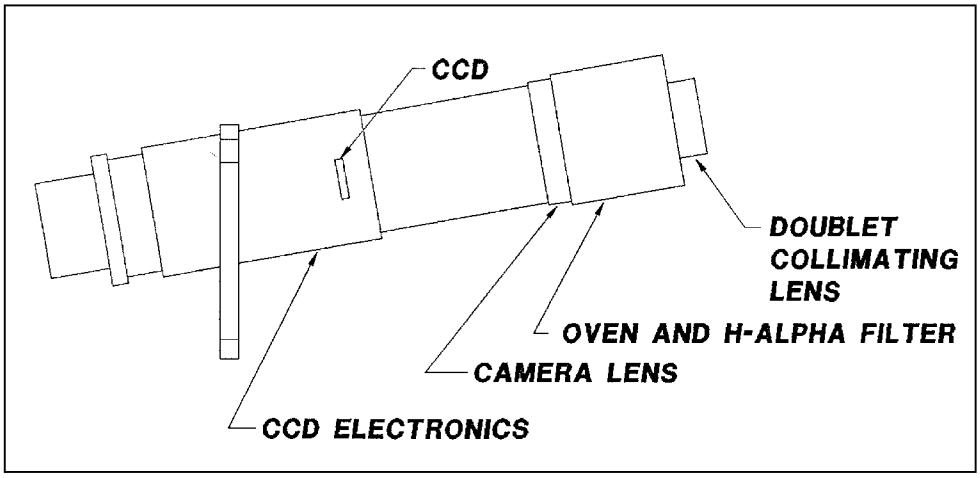

Figure 10. H-Alpha Camera.

III. PREFLIGHT CALIBRATION

A. Spectral Calibration (wavelength)

There are two types of calibrations needed to fully characterize a solar EUV instrument constructed with a telescope and a spectrometer with an imaging detector. The first is a wavelength or spectral calibration, identifying focused lines in the EUV in the imaging detector as a function of position as the data is recorded and readout from the CCD; the instrument profile will be determined from this data.

For this test, the telescope and its supporting section are removed and the detector, electronics, spectrometer and slit with the central bulkhead, are attached to a vacuum tank. A hollow cathode discharge lamp generates ionized He and Ne, producing radiation that exits the lamp through an open slit onto a reflecting ellipsoidal mirror, which then focuses the radiation onto the entrance slit of the spectrometer. The chamber has vacuum pumps to pump out itself and the spectrometer to a low pressure of 10^{-6} torr (10^{-5} torr during lamp operation when He-Ne gases are flowing into the chamber). See Figure 11.

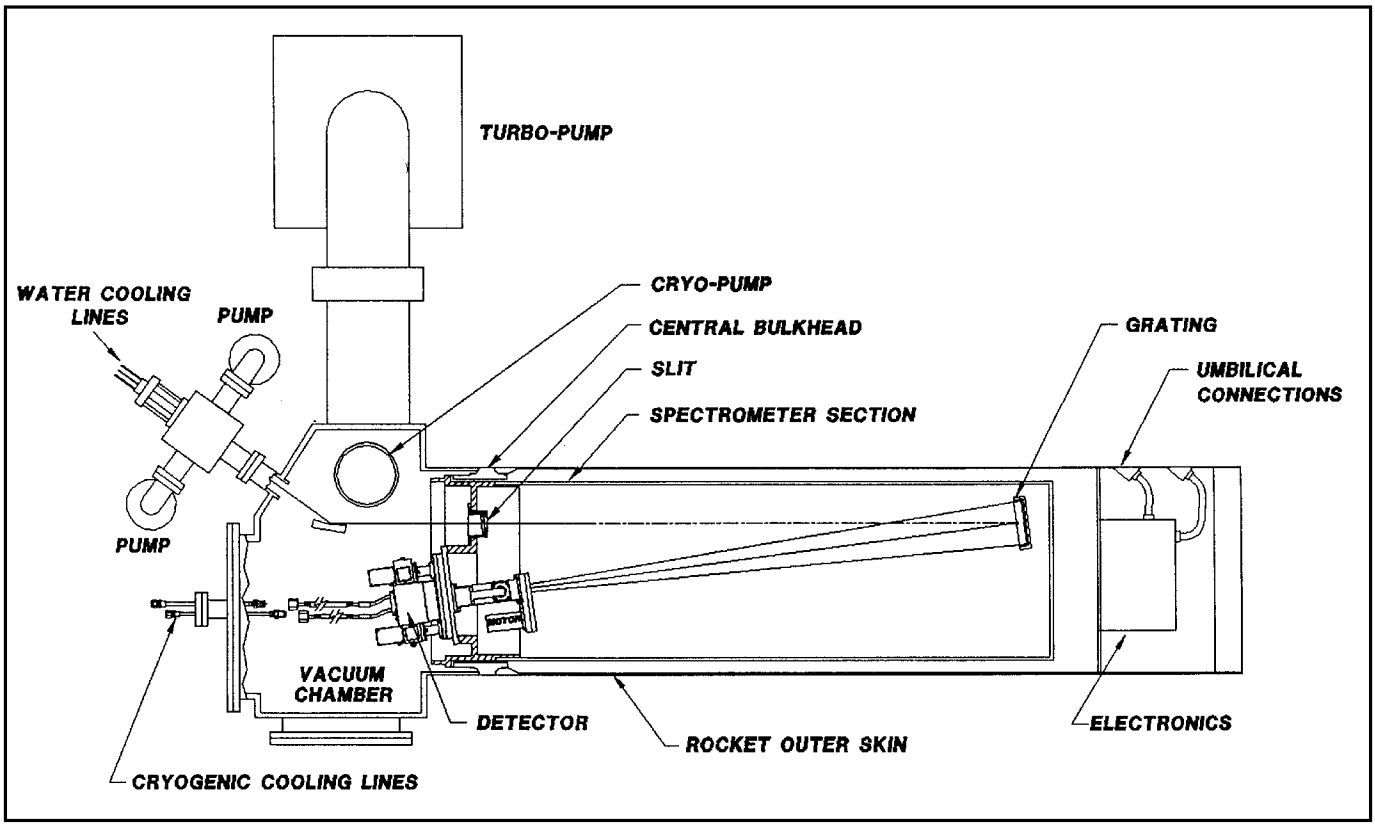

Figure 11. Calibration Chamber and Spectrometer Section.

An electrical discharge, nominally at 1750 Volts and 700 milliamps, is passed through the He-Ne gas mixture to produce spectral lines in the EUV. The He II line at 304 Å is very strong and at the short wavelength end of the wavelength range selected for the flight. The He II and many Ne II lines provide an excellent wavelength calibration throughout this wavelength range. A list of the emission lines produced by this laboratory lamp is listed in Table 6. We also list some impurity lines of oxygen and nitrogen, which might be found. See reference by Kelly and Polombo.

Table 6. Laboratory Calibration Lines (300 Å to 360 Å)

Identified He, Ne lines			Some impurity lines of oxygen and nitrogen that may also be present		
λ(A)	ion	comparative intensity (from Kelly)	λ(Å)	ion	comparative intensity (from Kelly)
301.12	Ne III	400	304.92	N III	500
303.782	He II	665	305.920	N III	500
308.56	Ne III	100	320.979	O III	600
313.05	Ne III	400	325.788	N III	20
313.68	Ne III	300	328.448	O III	500
313.92	Ne III	100	328.742	O III	450
320.392	He I	weak	330.26	N III	300
322.696	Ne III	-	345.309	O III	500
324.5686	Ne II		355.137	O III	300
326.5376	Ne II	40	355.293	O III	150
326.7855	Ne II	50	349.918	O III	100
327.6210	Ne II	20	355.333	O III	250
352.9549	Ne II	90	355.469	O III	250
353.2145	Ne II	30			
354.9620	Ne II	60			
356.8001	Ne II	50			
357.5346	Ne II	40			

As the lamp is operated with the He-Ne gas mixture, an exposure is recorded by the detector and its image stored in the GSE computer. Using Interactive Data Language (IDL) programs, a spectral plot of the resulting intensity vs. wavelength is made. Figure 12 shows such a sample laboratory spectrum, with wavelength identifications. The He II line anchors the short wavelength side, while Ne II lines dominate the spectrum on the long wavelength side. Once these lines are identified, it remains to position them exactly to get the coverage between the desired range of 298 Å to 354 Å. A slight change in the angle of the grating to the incoming beam moves the entire spectrum on the focal plane (face of the detector) so that the narrow section of the 304 Å lines is positioned at close proximity to pixel column 350 on the CCD. The position and wavelength identifications of the laboratory spectrum will be used to analyze the solar spectrum that was recorded by the same detector during the SERTS-97 flight.

This same laboratory setup is also used during adjustment of the spectrograph into its best spectral focus, accomplished by moving the grating toward or away from the slit. When the laboratory spectral lines are at their smallest or narrowest values at the center and at both ends of the spectrum, focus is achieved, and all components are then locked securely into position for flight.

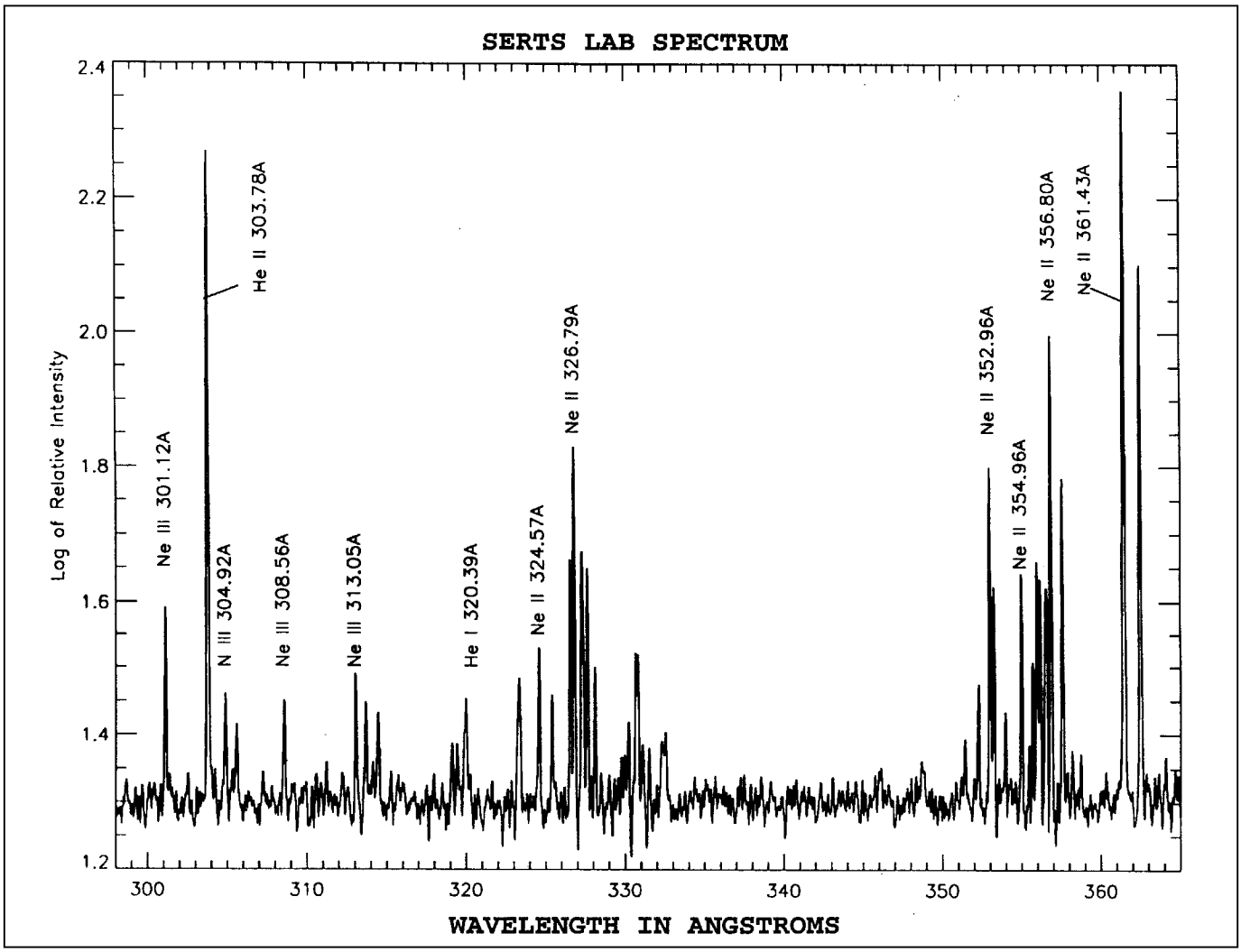

Figure 12. SERTS Lab Spectrum.

B. Absolute Intensity Calibration

The second type of calibration is an absolute intensity calibration, so that one can convert counts from the detector-readout into the number of EUV photons from the Sun striking the instrument. For this test, the complete SERTS experiment was sent to Rutherford Appleton Laboratory (RAL) in England, where it was installed in the same vacuum facility with the same EUV radiation source that was used in the original pre-flight calibration of the SOHO/CDS experiment. The EUV radiation source itself was specially developed by the Physikalisch-Technische Bundesansalt (PTB) in Germany.

This source standard is a hollow cathode glow discharge using He and Ne gases, which emits line radiation between 150 Å and 1500 Å. It produces a number of lines between 300 Å and 360 Å in our range of interest. The output of each line (photon flux) was determined by direct comparison to the calculable synchrotron radiation of the primary standard known as BESSY. The diverging radiation from the hollow cathode source is collimated by a Wolter Type II telescope used in reverse; i.e., the lamp radiation falls on the hyperbola and exits from the parabola. The output beam from this telescope is limited to a spot size of only 5-mm diameter, which is then directed onto the SERTS telescope surface. By moving the whole SERTS instrument or the source, we can expose many different parts of the SERTS telescope in order to simulate full-aperture illumination. To assure that none

of the incident radiation is blocked before reaching the detector, the spectrograph entrance aperture was removed for this test; its affect on the flight data can be easily included in the final calibration by geometric measurements of the aperture openings.

We now refer to the report published by PTB listed as reference #4, with authors J. Hollandt, M. Kuhne, M.C.E Huber, and B. Wende: "The photon flux from the lamp at any given line has an uncertainty of not more than 7%. The photon emission from the lines range from $6.3x10^5$ photon/s for the Ne III ion at 308.6 Å to $4.8x10^7$ photon/s for He II at 303.78 Å." There are twelve line-groups produced by this lamp with well-established absolute intensities in the SERTS bandpass. These gave us the input flux values needed to do the absolute calibration for our SERTS-97 instrument. The first analysis will appear soon in publication by Roger Thomas et al.; a preliminary analysis was presented at the January 1998 AAS meeting in Washington, D.C. This absolute intensity calibration was then later transferred to the SOHO CDS and EIT instruments through observation of the same feature on the Sun during the SERTS-97 flight on 1997 November 18 (see Figure 24). After completing the absolute intensity calibration at RAL, the SERTS experiment is sent back to GSFC.

IV. ASSEMBLY AND TEST OF THE SERTS AT GODDARD SPACE FLIGHT CENTER

The SERTS experiment section arrives at Goddard Space Flight Center. The telescope section is removed; the GSE control box is connected via the umbilical connection to the experiment and the battery pack is removed and attached to the GSE as a backup should lab power fail. Vac ion power is applied to run the vac ion pumps. The aperture-disk is reinstalled. The experiment is attached to the laboratory vacuum tank with the hollow cathode discharge lamp. The same spectral calibration runs were made as in part IIIA- spectral calibration of the instrument. This identifies again the positions of the wavelengths on the detector, the focus of the lines, and checks the performance of the electronics. Next, the pointing of the sensor eyes is verified in relation to the telescope axis by using an auto-collimator that focuses on the front faces of the telescope and the sensing eyes.

The data from these tests are analyzed and, when each section of the experiment meets the desired performance, the telescope section is attached to the spectrometer section, the battery pack is connected to the electronic section, and the shutter door is mounted onto the telescope section. The experiment is then boxed and shipped to White Sands Missile Range, New Mexico. During shipment, the vac ion pumps are continuously operating to keep the detector at 10^{-6} torr.

V. PREFLIGHT TESTS AT WHITE SANDS MISSILE RANGE

A. Functional Tests – Launch Sequence Bench Tests – All Payload Components

1. Pre- T & E horizontal functional tests

When the experiment and associated equipment arrives at WSMR, building N200, the battery pack is removed from the experiment and connected to the GSE as a back-up power source. The GSE is connected to the experiment by cables through the umbilical connectors to provide power via the umbilicals to the vac ion pumps to keep the detector at 10^{-6} torr. The turbo vacuum pumping station is connected to the experiment and pumps it down to 10^{-4} torr to check for any leaks. The following checks and tests are made: sensor wiring, mechanical and electrical interfaces, telemetry, command link practice, telescope alignment with slit, and the telescope alignment with the LISS and the MASS (pointing sensors) is measured.

The experiment is assembled with the telemetry section, the S-19 section, the SPARCS section, the Orsa and Ogive sections in a horizontal configuration, on adjustable movable tables. Ground support equipment for certain sections is connected. The payload is run through its flight-timer sequence, which simulates each event during the

flight. The payload is tested when the experiment is at atmospheric pressure and again when the experiment is under vacuum. Each section must meet the electrical and mechanical performance requirements. After these tests are completed, the payload, fully assembled, with the battery pack reattached electrically through the umbilical connectors and running the vac ion pumps, is moved to the VAB (vehicle assembly building). Figure 13 shows the payload fully assembled. (Figures 13 and 17 are reproduced from Wallops Flight Facility report TM-98/4302).

2. T & E tests in VAB

The T & E personnel perform the following tasks at the VAB: initial weight and center of gravity, bend tests, check spins, measure joints, roll MOI, pitch/yaw MOI, vibration tests, and final weight and center of gravity.

3. Post T& E tests

The payload arrives back at building N200. The GSE is attached to it by the umbilical lines, and the battery pack is attached to the GSE as a back-up. The Post T & E tests are basically the same as those that were performed during the pre-T & E horizontal functional tests. The telescope and Sun sensors alignment is checked again. The electrical and mechanical tests are made to verify a successful performance. The payload makes its journey to the launch site with the battery pack powering the vac ion pumps through the umbilical connection.

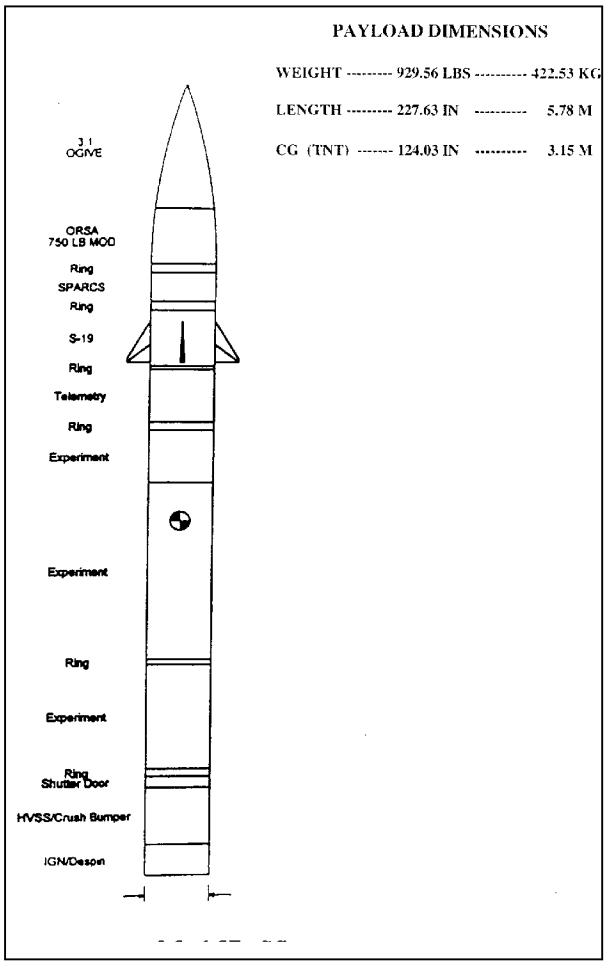

Figure 13. SERTS 36.167–GS Payload Configuration.

VI. ROCKET CONFIGURATION FOR FLIGHT

A. The payload is delivered to the launch gantry and rail, and mounted in a horizontal position.

B. The payload is assembled to the Black Brandt rocket motors and Terrier booster. Figure 14 shows the overall rocket assembly.

C. The assembled rocket is raised to the vertical position. The battery pack remains attached and powers the vac ion pumps on the detector.

D. The screws at the interface between the payload and the rocket motors are tightened to specifications; the rocket is lowered back to its horizontal position.

E. The battery pack is disconnected; the umbilical and land-lines are connected between the payload, GSE, and computer in the Blockhouse.

F. Upon authority of the payload manager, the GSE is turned on, and the vac ion pumps are powered up.

G. The experiment is connected to the portable turbo vacuum system, and to the CCD cooling lines from the LN_2 reservoir.

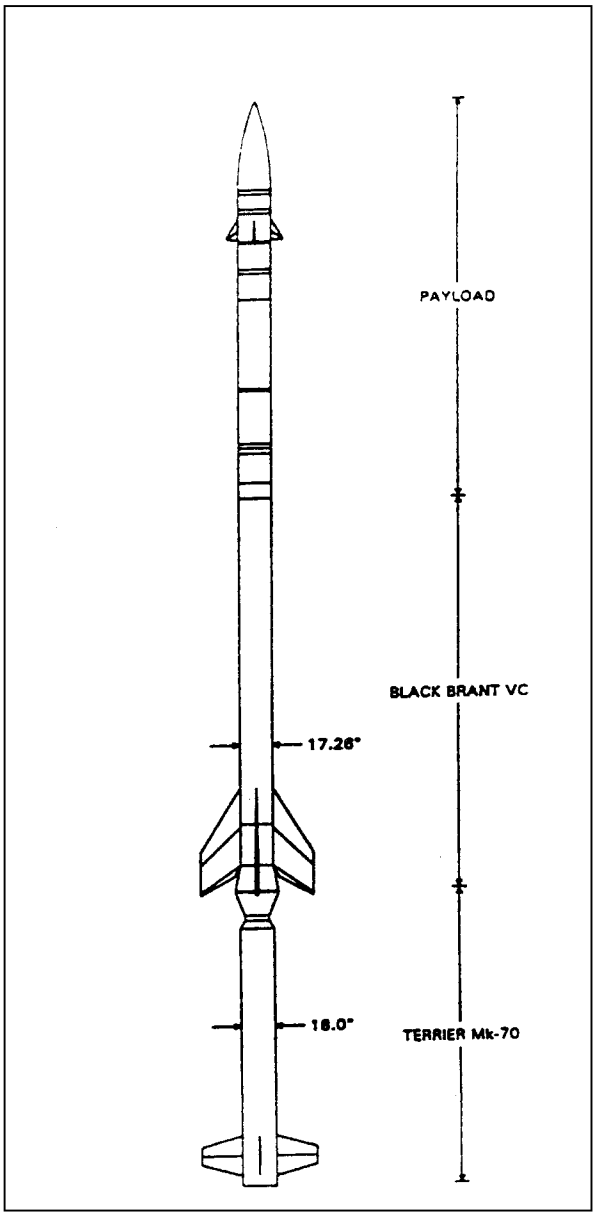

Figure 14. Terrier Black Brant (MOD 2) 36.167 GS Vechicle Configuration.

Figure 15 shows the fully assembled rocket with the experiment as a breakaway section. The vacuum pump-out port, the cryogenic connector flange, and the umbilical connectors are indicated for clarity. Figure 16 is a view of the fully assembled rocket in the horizontal position, with the ground supported turbo-vacuum system and cooling lines attached.

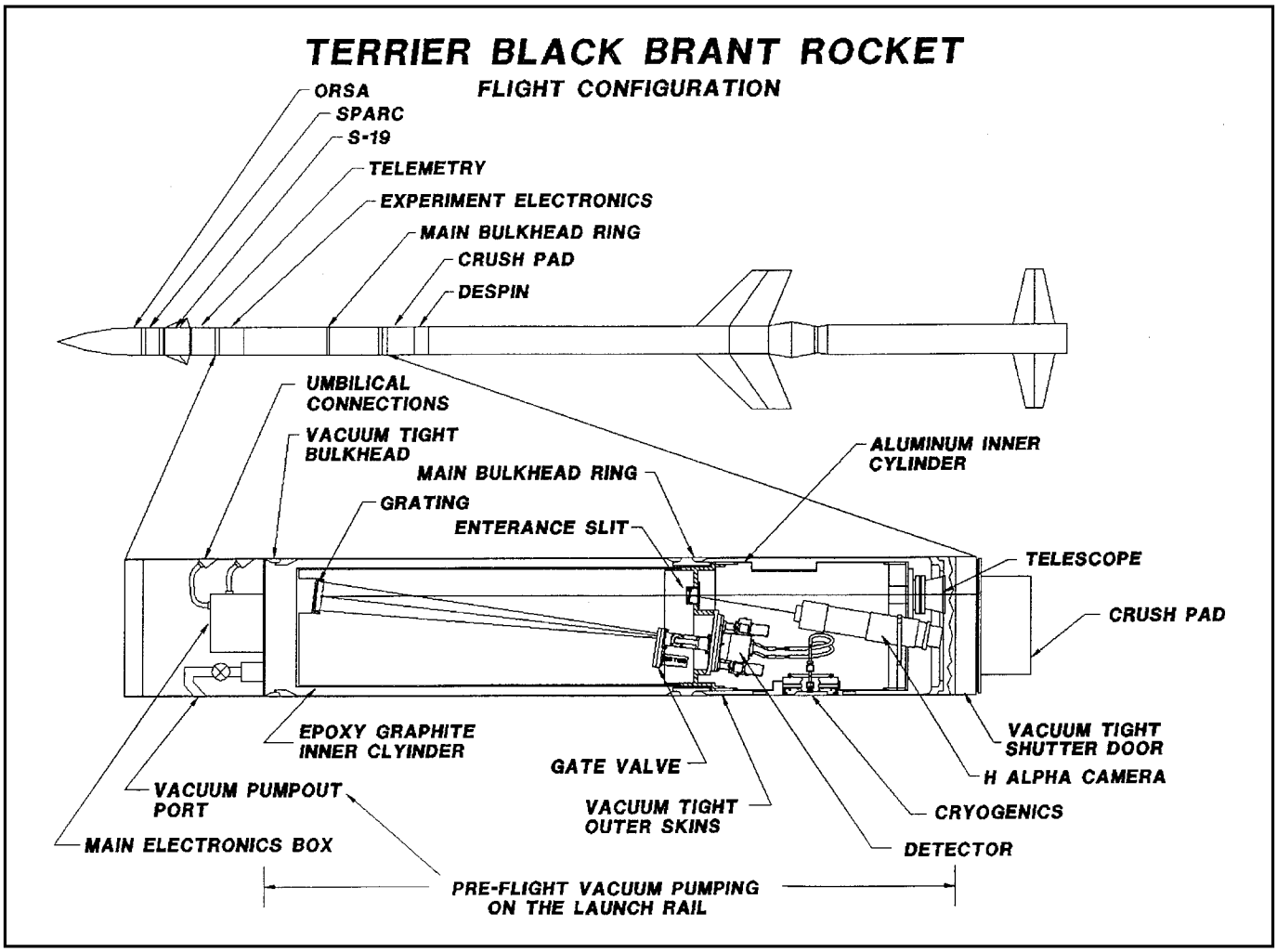

Figure 15. SERTS Experiment.

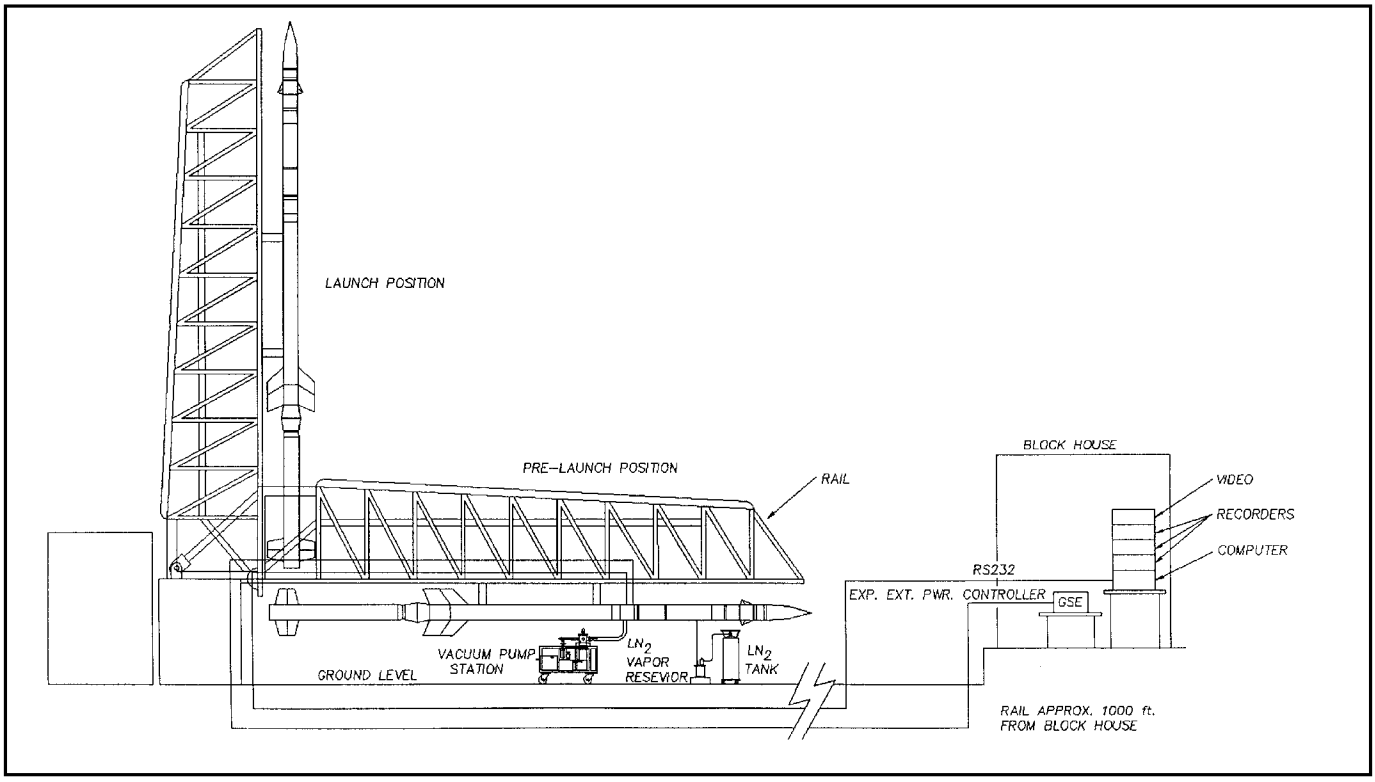

Figure 16. SERTS on ATHENA Launching Rail and Block House Setup for launch.

VII. FLIGHT OF SERTS-97

A. Preliminary Countdown Activity

During launch countdown, the experimenter, using the GSE in the blockhouse, supplies power to the vac ion pumps and electronics, and monitors the electronic status of the components in the experiment via the umbilicals. The vac ion pump current is monitored to determine the vacuum in the detector; the temperature of the CCD is measured and displayed via an RS-232 link back to the computer at the blockhouse. The Hα oven power is supplied by the GSE, and the position of the valves is displayed on the GSE console.

Two days before launch (T-2 days), the portable turbo-vacuum system is turned on to pump out the experiment through a pump-out valve. Each day the experiment is pumped down and then backfilled with dry LN_2 gas. On the day of the launch, pump down begins 4 hours and 30 minutes before launch and at T-1 hour and 20 minutes, the vacuum system is separated from the experiment. The experiment pressure is approximately 1-2 μm at launch.

The CCD cooling begins on the day of the launch when the vacuum system has pumped the experiment down to 50 μm. The CCD temperature is –40°C at T - 1 hour & 20 minutes. At this time the GSE console is powering the vac ion pumps on the detector. The status is reviewed on all systems. At T - 1 hour & 10 minutes, the cooling system is separated from the experiment and the vac ion pumps are turned off. All console GSE power is turned off. No electrical power is permitted at this time to be sent to the experiment. All vehicle power is off. At T-60 minutes, all personnel except for the rocket arming crew, clear the launching site.

The rocket is then armed.

B. Final Countdown

At T-40 minutes, upon authority of the payload manager, GSE power is turned on. Then vac ion power is turned on. The temperature of the cooling block is checked. The CCD temperature is displayed by the computer monitor in the blockhouse via the RS-232 umbilical link through the land-lines. As the launch countdown continues –

AT T-30 minutes, the gantry is raised from its pre-launch horizontal position to the vertical launch position (see Figure 16); the umbilicals remain attached (although not shown so in Figure16), providing GSE power to the vac ion pumps, and connections to monitor the detector temperatures by the experimenter in the blockhouse.

Time	Event	Responsibility
T-300 sec	Check vac ion pump current (pressure).	Exp.
T-120 sec	Power to all systems switched to internal battery power in the Rocket; vac ion pumps are powered by the internal batteries.	Inst. Timer
T-110 sec	GSE vac ion enables off. Vac ion current monitored by GSE.	Exp.
T-90 sec	Project manager verifies all systems go.	
T-10 sec	GSE power off.	Exp.
T-0	**Rocket booster firing, lift off, umbilicals are separated from the rocket.**	**Launch Crew**

Experiment Status at T-0

Experiment Power	=	internal rocket batteries
CCD temperature (pin)	=	0 °C
Detector Vac Ion Pumps Pressure	=	$<5.0 \times 10^{-6}$ torr
Experiment Vacuum	=	1-2 μm
Hα camera	=	off
Hα oven	=	on
Detector bypass valve	=	open
Detector door	=	closed
Detector electronics	=	off
GSE power	=	off

Time	Event	Responsibility
T + 6.2 sec	Terrier Burnout	
T + 12.0 sec	Black Brant Ignition	
T + 18.0 sec	S-19 Canard Decouple	
T + 44.4 sec	Black Brant Burnout	

T + 48 sec	Vac. Ion Enable Exp. Command ON	- Instr. Timer
T + 50 sec	Exp. Main Bus Power & Hα Camera ON	- Instr. Timer
	Detector electronics on, CCD in flush mode	
	Housekeeping ON	
	Temp. monitor ON	
T + 57 sec	Yo-Yo Despin	- PSL Timer
T + 61 sec	Payload Separation	- PSL Timer
T + 62 sec	SPARCS Enable	- Instr. Timer
T + 64 sec	S-19 Gyro Cage, Open Shutter Door	- Instr. Timer
	(Exp. Door) at 295,000 feet (54.9 miles)	
	Pressure 7.9×10^{-4} mm	
T + 74 sec	Nose Cone Eject	- PSL Timer
T + 82 sec	Start RS-232 Monitor	- Exp.
T + 86 sec	Bypass Valve Closed	- Instr. Timer
T + 94 sec	Detector Door OPEN	- Instr. Timer
T + 99 sec	IIC Bus Power ON	- Instr. Timer
	(HV on detector)	
T + ~101 sec	Exp. Start (command from ASCL)	- Command Link
	This starts observing sequence at	
	550,000 feet (104 miles)	
T + 107 sec	Exp. Back-up start pulse	- Instr. Timer
T + ~165 sec	Send Pitch Offset	- Cmnd. Link/Exp.
	(Roger Thomas from ASCL)	
T + 514 sec	Shutter Door Closes – at 420,000 feet	- Instr. Timer
	(79.54 miles) Pressure 4×10^{-6} mm	
	SPARCS Inhibit	- Instr. Timer
	IIC Bus Power OFF	- Instr. Timer
	(HV OFF)	
T + 515 sec	Detector Door CLOSE	- Instr. Timer
T + 519 sec	Bypass Valve OPEN	- Instr. Timer
T + 520 sec	Switch to SCS3 to begin testing	- ASCL
T + 530 sec	Spin-Up Start	- Instr. Timer
T + 540 sec	Spin-Up Stop	- Instr. Timer
T + 552 sec	S-19 OFF	- Instr. Timer
T + 780 sec	Exp. Main Bus Power OFF	- Instr. Timer
	Exp. Hα Camera OFF	- Instr. Timer
	Vac. Ion Exp. Enable OFF	- Instr. Timer
T + 782 sec	Exp. External	- Instr. Timer
	Exp. Hα Filter Power OFF	- Instr. Timer
	Valve & Detector Door Power OFF	- Instr. Timer
	Thermistor Power OFF	- Instr. Timer
	Vac. Ion Power OFF	- Instr. Timer
	Vac. Ion Enable OFF	- Instr. Timer
	2279.5,2215.5 MHz Transmitters Power OFF	- Instr. Timer
T + 784 sec	Vac. Ion Enable Exp. Command OFF	- Instr. Timer
T + 819 sec	Timer #1 & #2 End of Run	- Instr. Timer
T + 900 sec	TM LOS	- Instr. Timer

VIII. FLIGHT PERFORMANCE

The actual flight path had an apogee (maximum altitude above sea level) of 332 kilometers (206 miles). The actual flight path vs. time is presented in Figure 17, reprinted from Wallops Flight Facility Report TM-98/4302. The actual flight altitudes vs. time are so close to the predicted altitudes that the deviations will have no effect on the performance of the experiment.

The experiment was recovered in excellent condition.

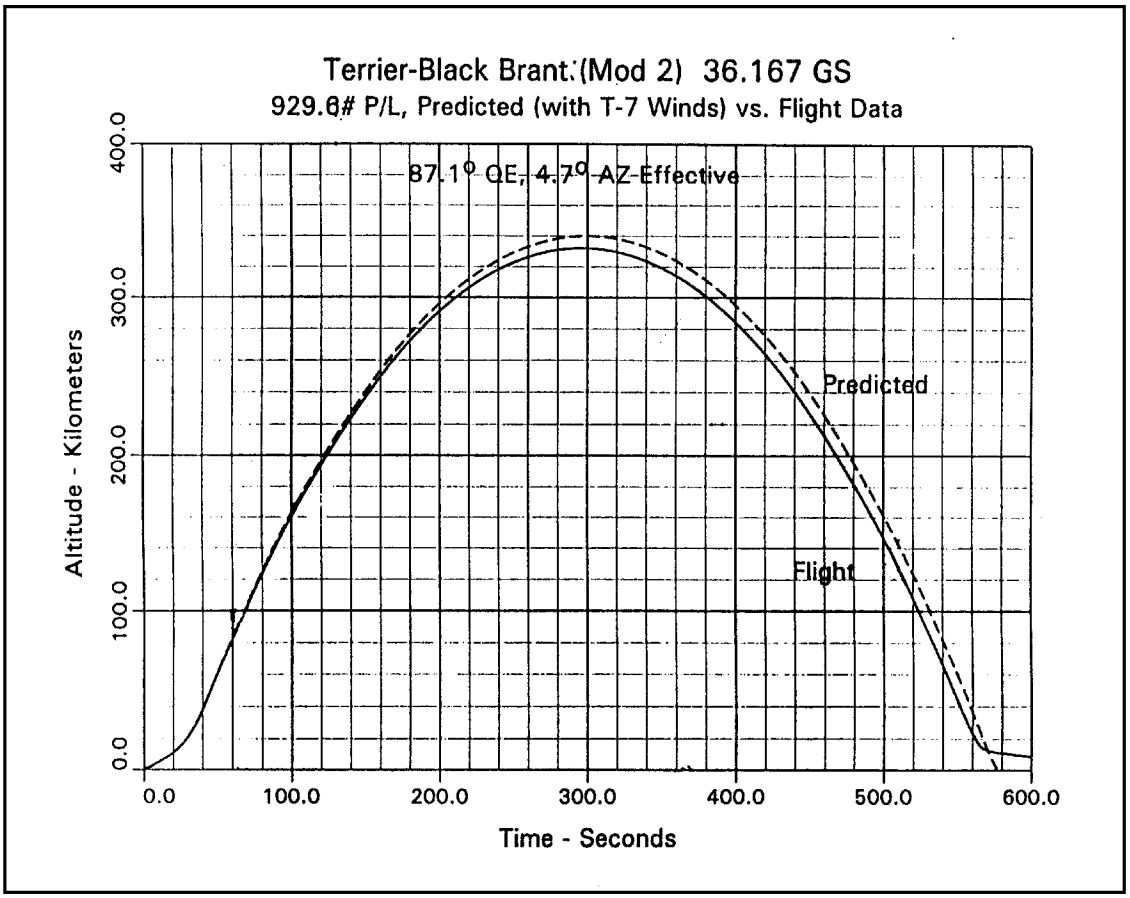

Figure 17. Flight Trajectory

The observing sequences started at an altitude of 177 km (581,000 feet) at T+107 seconds by the experiment back-up start pulse. At this time, the experiment was in the 1st pointing position. Refer to Figure 23. The background image of the full sun is at 304 Å and was recorded by the EIT instrument on the SOHO satellite. SERTS is pointed so that one entrance lobe is positioned to cover the target active region. The smaller rectangular box is the coverage of the same active region at the same time by the CDS instrument on SOHO.

Four images were recorded with integration times of 30, 10, 3, and 1 second at the 1st pointing position. SERTS then moved to the 2nd pointing position, where four groups of images were recorded. Each group contained 3 images with integration times 30, 10, and 3 seconds. The fifth and last group contained recorded images with integration times of 1, 10, and 60 seconds.

The 2nd pointing position can best be demonstrated by referring to Figure 24. The narrow-slit part of the aperture is superimposed over the active region between two bright areas. The spectral line list presented in Table 1 was generated from this pointing position. The CDS instrument observed a substantial area overlapping the SERTS slit coverage, allowing for cross-calibration between the two instruments. Figures 23 and 24 were generated by William Thompson from data taken at the same time by the CDS and EIT experiments aboard the SOHO satellite and by the SERTS-97 experiment during its flight.

IX. PRELIMINARY RESULTS

There are four categories upon which we are concentrating our efforts to analyze the data. The first is to generate an absolute calibration curve for SERTS-97 to convert the recorded detector responses into absolute intensities from the Sun at each measured wavelength. (See Section III-B.) This will enable us to cross-calibrate to the SOHO-CDS and EIT experiments. A paper by Thomas et al. was presented at the AAS meeting in Washington, D.C. on 1998 January 9 with preliminary results. The calibration analysis is nearing completion, and final results will be published in the near future by Thomas et al. The second effort is to generate a spectral line list, which we have partially completed as shown in Table 1. The line list was generated from data recorded during the 2nd pointing position of the instrument, when the narrow-slit was on the target active region. The third effort is an analysis of the images taken during the 1st-pointing position (see Figure 23). The last effort will be to check the electronics and all functions of the electro-mechanical parts of the instrument.

A list of selected ions along with their corresponding log Tmax values is presented in the Brosius et al. reference in the Astrophysical Journal 477: 969-981, 1997 March 10. Comparing the Brosius list to our list in Table 1 (SERTS-97 flight), we find the same wavelengths for these selected ions that are identified in the 298 Å-354 Å range. They are listed in Table 7 with log Tmax values.

Table 7. Ion vs Temperature

Ion	Log Tmax	λ(Å)
Fe X	5.98	345.17
Fe XI	6.06	341.14, 352.68
Fe XII	6.14	338.27, 346.85, 352.12
Fe XIII	6.20	318.12, 320.80
Fe XIV	6.27	334.17, 353.82
Fe XV	6.33	327.04
Fe XVI	6.43	335.40
Fe XVII	6.60	338.27
He II	4.67	303.781
Si XI	6.20	303.32
Ni XVIII	6.52	320.56
Ca XVIII	6.76	302.167

The Tmax for this large number of ions indicate plasma temperatures T of $.96 \times 10^6 < T < 5.8 \times 10^6$ K at the 2nd pointing position, when the active region was in the center of the slit (Figure 24). The ratio of the full-line intensities, taken from Table 1, between Fe XVI (335.4 Å) and Fe XIV (334.17 Å) is equal to R and is substituted in the formula $\log T = a_0 + a_1(\log R) + a_2(\log R)^2 + a_3(\log R)^3$ at densities of 10^9 and 10^{10} cm^{-3}. $R = I_{335.40}/I_{334.17} = 3615/387.5 = 9.33$; $\log R = .970$. These wavelengths are close together so that no instrumental throughput correction is needed. For each density, a_0, a_1, a_2, a_3 is obtained from Tables IX and X of Brosius et al. September (1996). See Table 8 for our results.

Table 8. Calculated Temperatures from Ratio of FeXVI/FeXIV

Density	a_0	a_1	a_2	a_3	logT	T (K)
10^9 cm^{-3}	6.237	.111	.00875	.00165	6.355	2.27×10^6
10^{10} cm^{-3}	6.217	.108	.00762	.00180	6.330	2.14×10^6

The resulting temperatures are close enough to indicate that density is not a factor when using the ratio of these lines to calculate temperature.

We also have calculated densities by line-intensity ratios from the same ion, using lines that are not affected by temperature. Those selected for this study come from Brosius et al. (Astrophysical Journal Supplement Series106: 143-164, 1996). Table 9 is a tabulation of the wavelengths, ions, SERTS-97 integrated detector-response ratios, calibration corrections, solar intensity ratio and the resulting electron densities. The preliminary calibration curve correction is taken from an efficiency curve generated by a line-ratio method from SERTS-91 data, which had similar optical components. A more definitive efficiency curve for SERTS-97 is in preparation and will be published soon.

Table 9. Calculated Electron Density from Fe Ratios

λ_1/λ_2	Ion	SERTS Response Ratio	x	Calibration Curve = Correction	Solar Intensity Ratio	Electron Density
353.81/334.17	Fe XIV	85.7/387.5		2.066	.457	5.0×10^9
338.28/352.12	Fe XII	33.7/86.3		.598	.234	6.3×10^9
318.11/348.19	FeXIII	26.7/97.2		.892	.245	2.5×10^9

The one-second exposure, taken at the 1st pointing position, gives us images of the active region selected by the lobe part of our aperture (see Figure 23). There are two distinct bright spots, which are observed at 304 Å (He II) and at 335 Å (Fe XVI). The morphology at these two wavelengths can be observed and compared. A contour image is presented with 335-Å intensity-contours superimposed on the 304-Å image. It is illustrative to generate 3-dimensional plots of the 304 Å and the 335 Å patterns of He II and Fe XVI emission, respectively, in X and Y with the Z-axis as intensity. Figure 18 is the 3-D plot of the 304-Å intensity, and Figure 19 is the corresponding 2-D contour plot obtained by projecting the intensity onto the X-Y plane. Figure 20 is the 3-D plot of the 335-Å intensity, with Figure 21 the projection onto the X-Y plane.

From these plots and contours, we find strong support of an earlier SERTS result. Jordan et al. (1993) argue on the basis of prior SERTS spectra that electron collisional excitation dominates the formation of the 304 Å line in the quiet Sun, and probably plays a significant role in active regions as well. Their argument uses the Fe XVI 335 Å line as a proxy for coronal radiation that drives the competing mechanism, photoionization-recombination, often called simply 'p-r.' This procedure was justified by reference to earlier Skylab work (Withbroe and Noyes, 1976), and has received further support from a recent SERTS-Yohkoh study (Falconer et al., 1998). If the Fe XVI 335 Å

line is a good proxy for coronal radiation, as indicated by the above studies, and if the p-r mechanism is in fact the dominant 304 Å line-formation mechanism, we would expect its intensity to vary approximately as the intensity in the 304 Å line. That it does not is clearly illustrated in Figures 19-21.

The easiest way to see this is by comparing the 2-D intensity contour plots of Figures 19 and 21. We are immediately struck by the fact that the locations of brightest intensity in the 304 Å and 335 Å lines are *reversed*! This is exactly opposite what we would expect if p-r were the dominant line formation mechanism for the 304 Å line. Also, the relative areas of intense radiation in the two lines are reversed, again opposite what we would expect under p-r conditions. And these results apply primarily to active region intensities, where p-r is more likely to have a significant effect; in the quiet Sun, its effect is even less. This is strong support for the electron collisional excitation formation of the 304Å line over most of the solar atmosphere.

Finally, the same result can be seen in Figure 22 alone, where we have plotted the 335 Å contours on top of a color plot of the 304 Å intensities. The scale is different from that of Figures 18 – 21, but the result is the same, as it must be since we are plotting the same data. It is perhaps easiest to see the relationships between Figures 18 - 22, if all the figures are viewed from the left side.

COLOR FIGURES 18-24

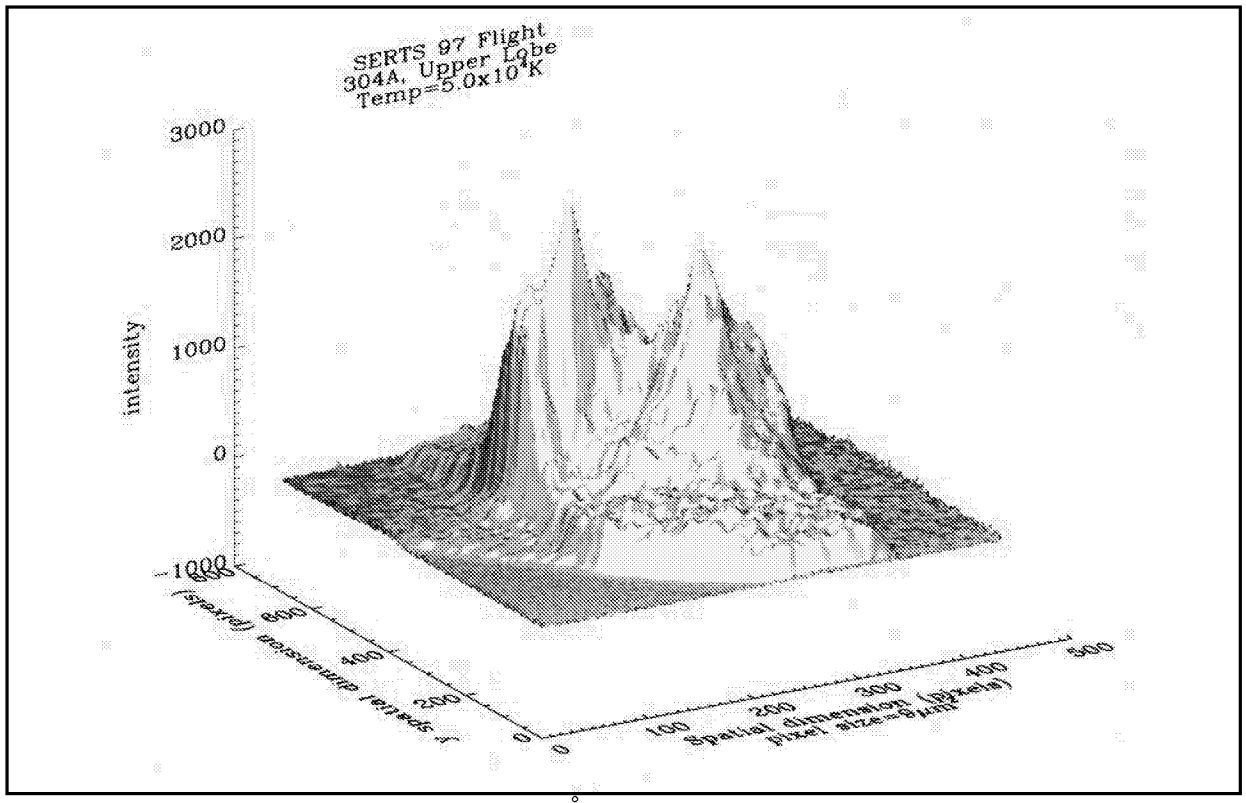

Figure 18. 3D plot of 304Å lobe image–intensity vs. x and y.

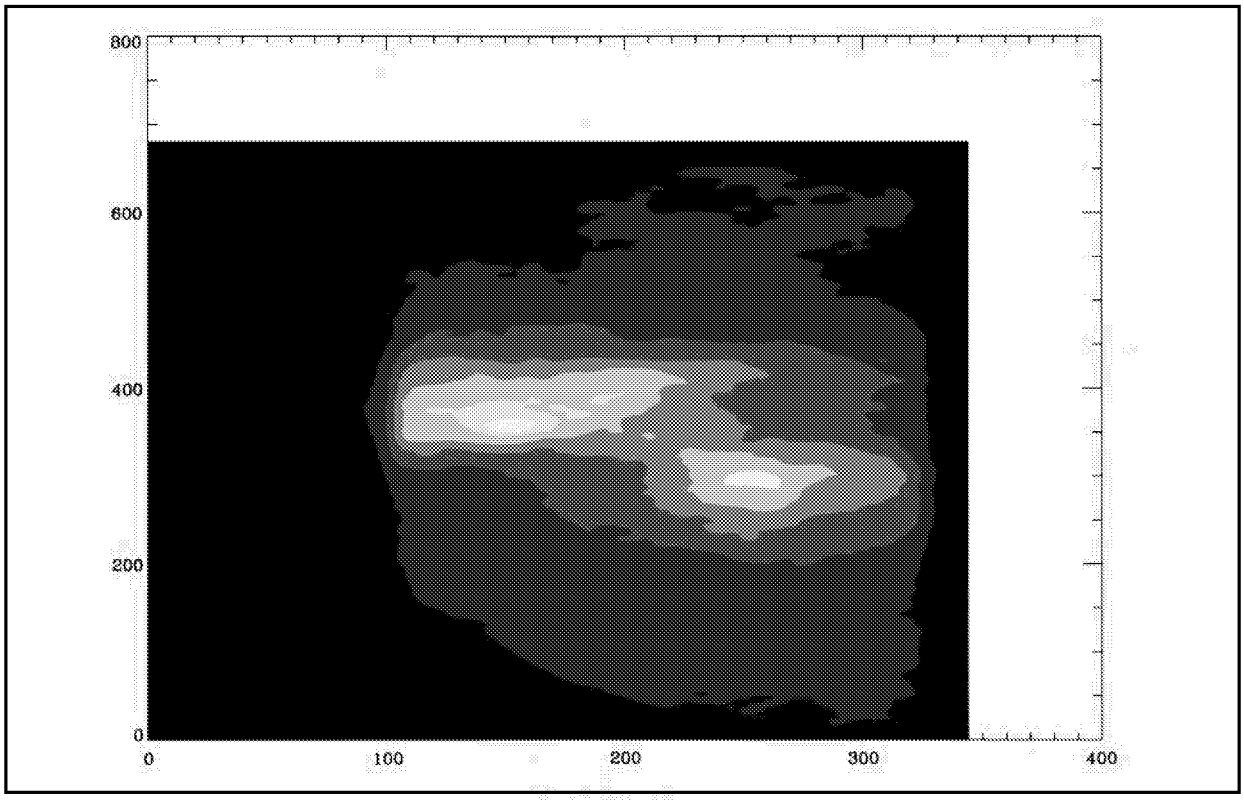

Figure 19. 304Å contour plot of intensity of lobe projection on the xy plane.

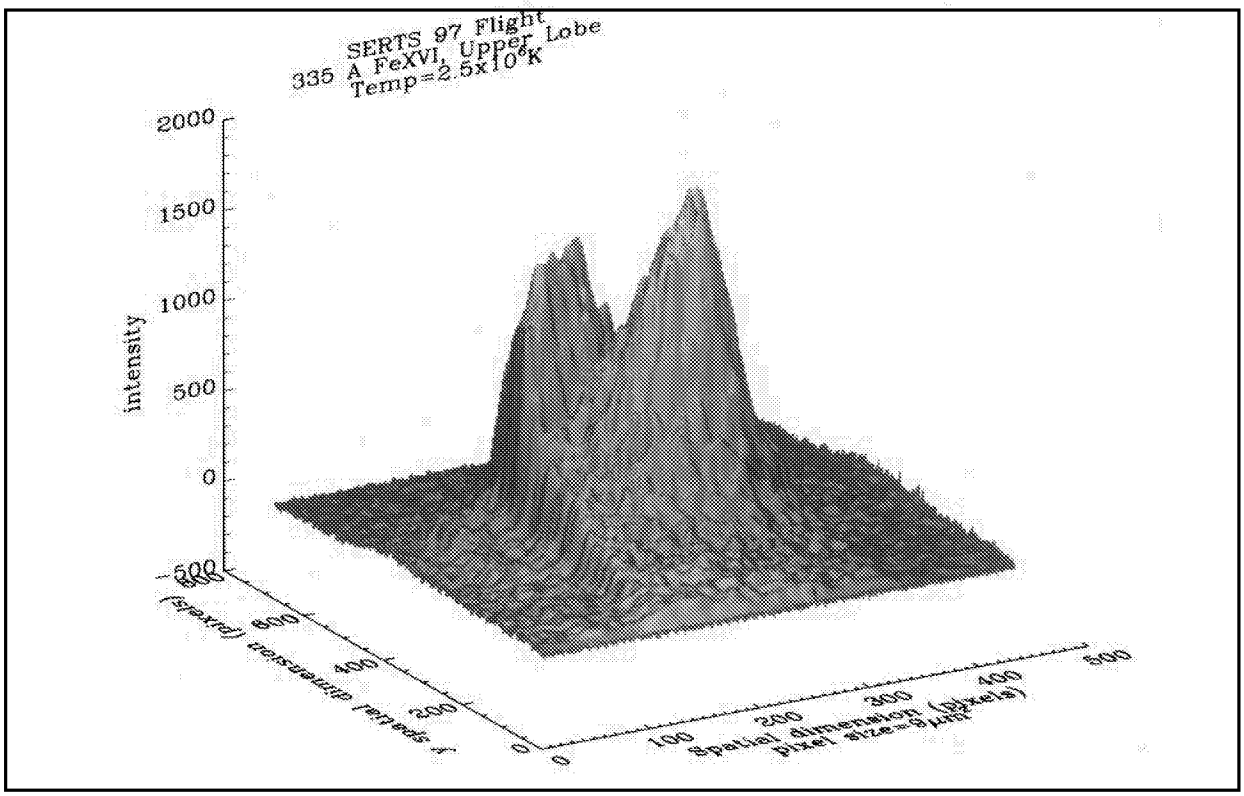

Figure 20. 3D plot of 335Å lobe image–intensity vs. x and y.

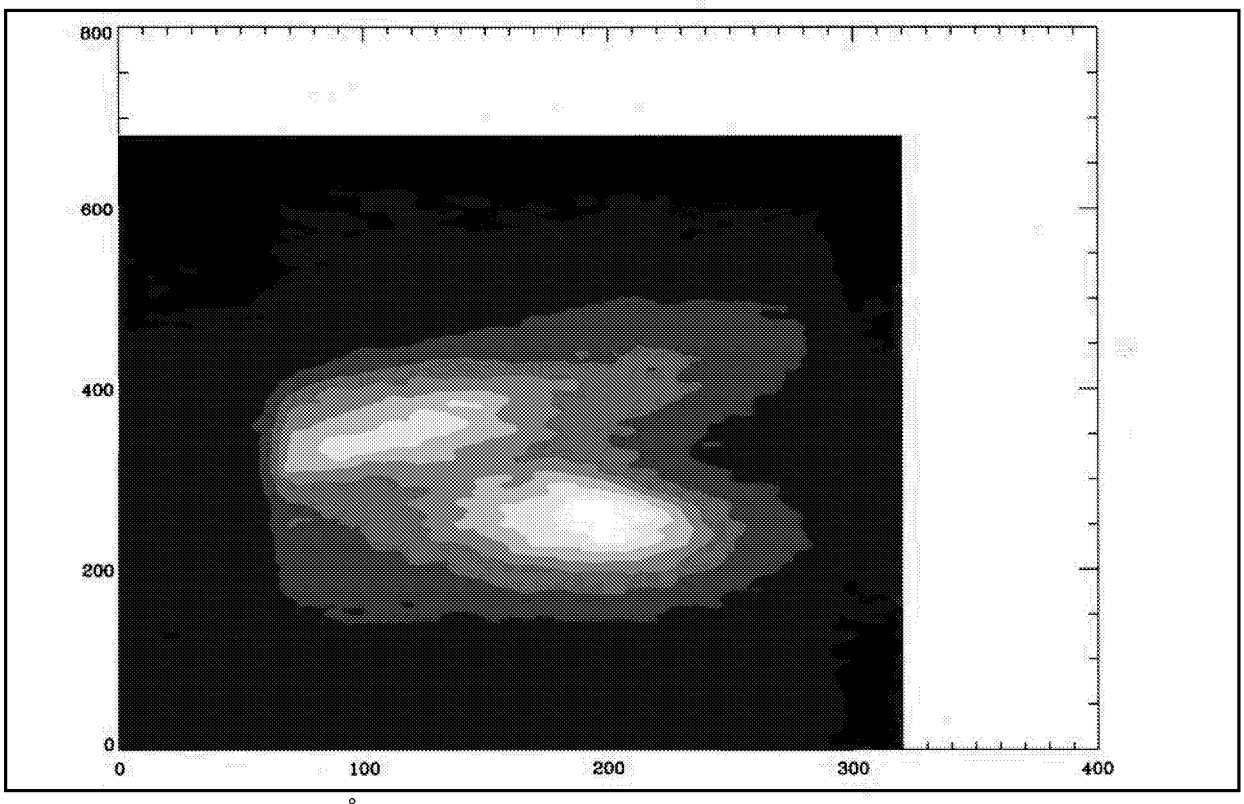

Figure 21. 335Å contour plot of intensity of lobe projection on the xy plane.

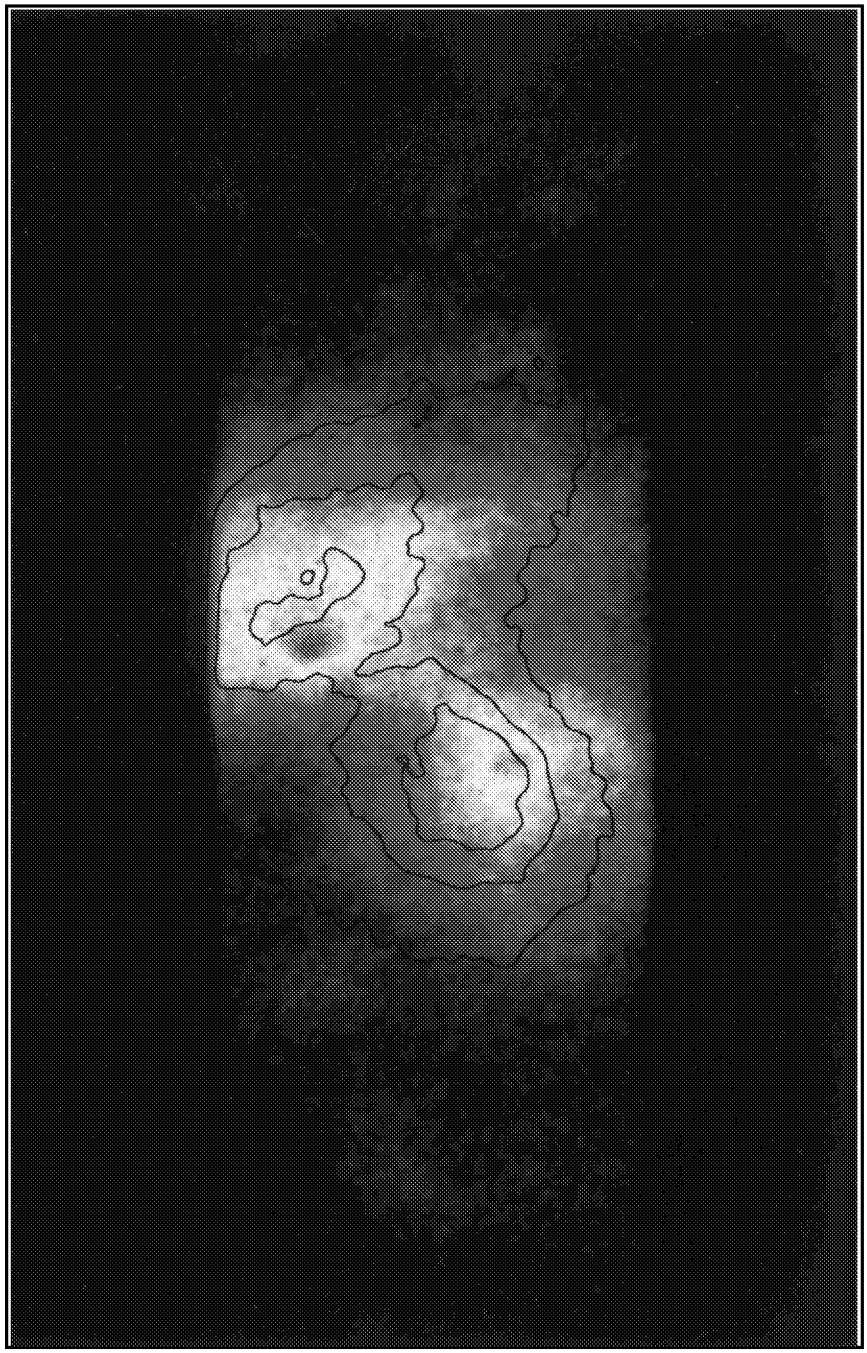

Figure 22. 335Å contour plot on top of the color plot of the 304Å intensity (lobe of the aperature on the active region). See Figure 23.

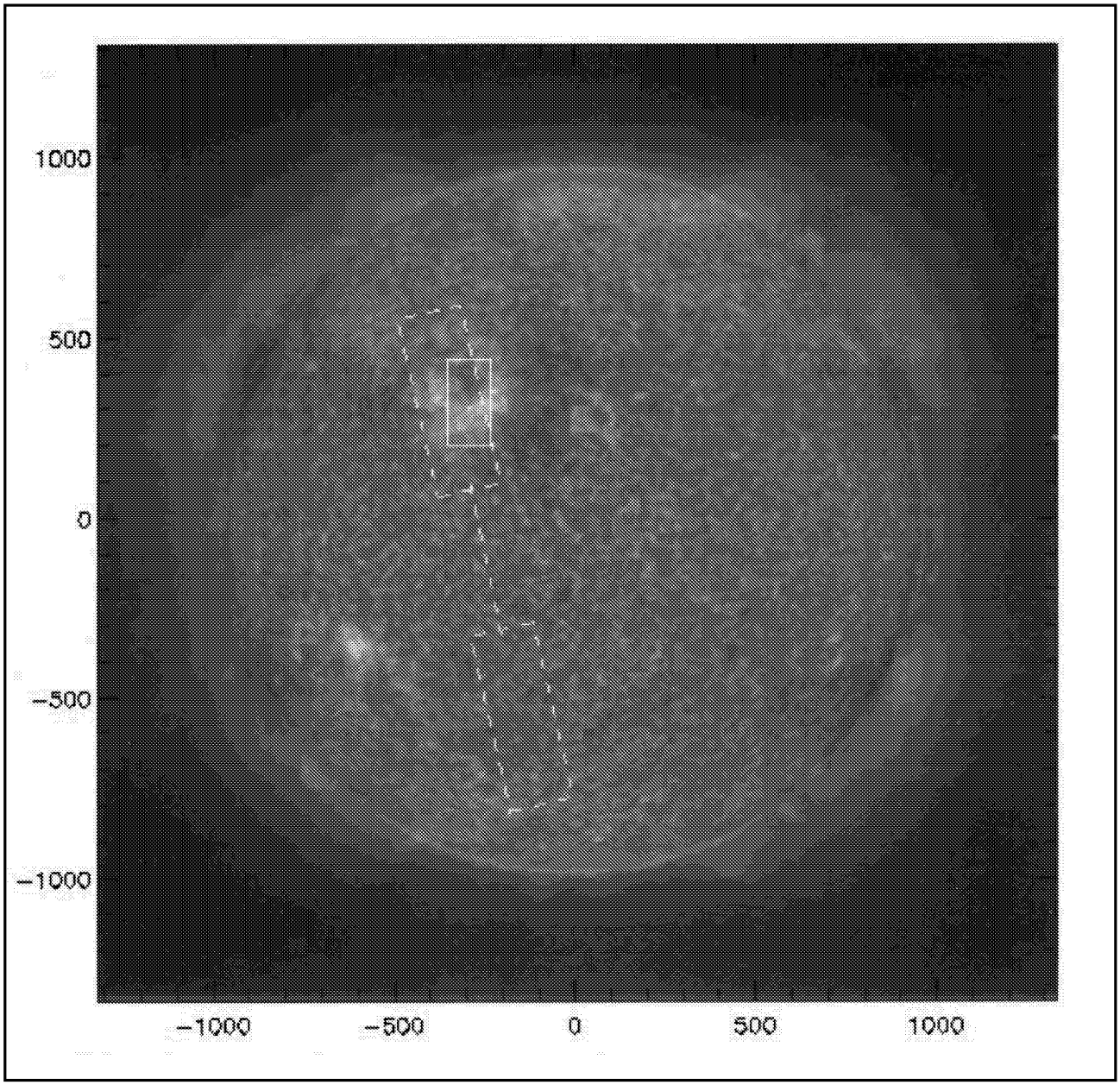

Figure 23. SERTS pointing position 1 (dotted line) showing lobe alignment over active region. Small box is CDS coverage of same active region.

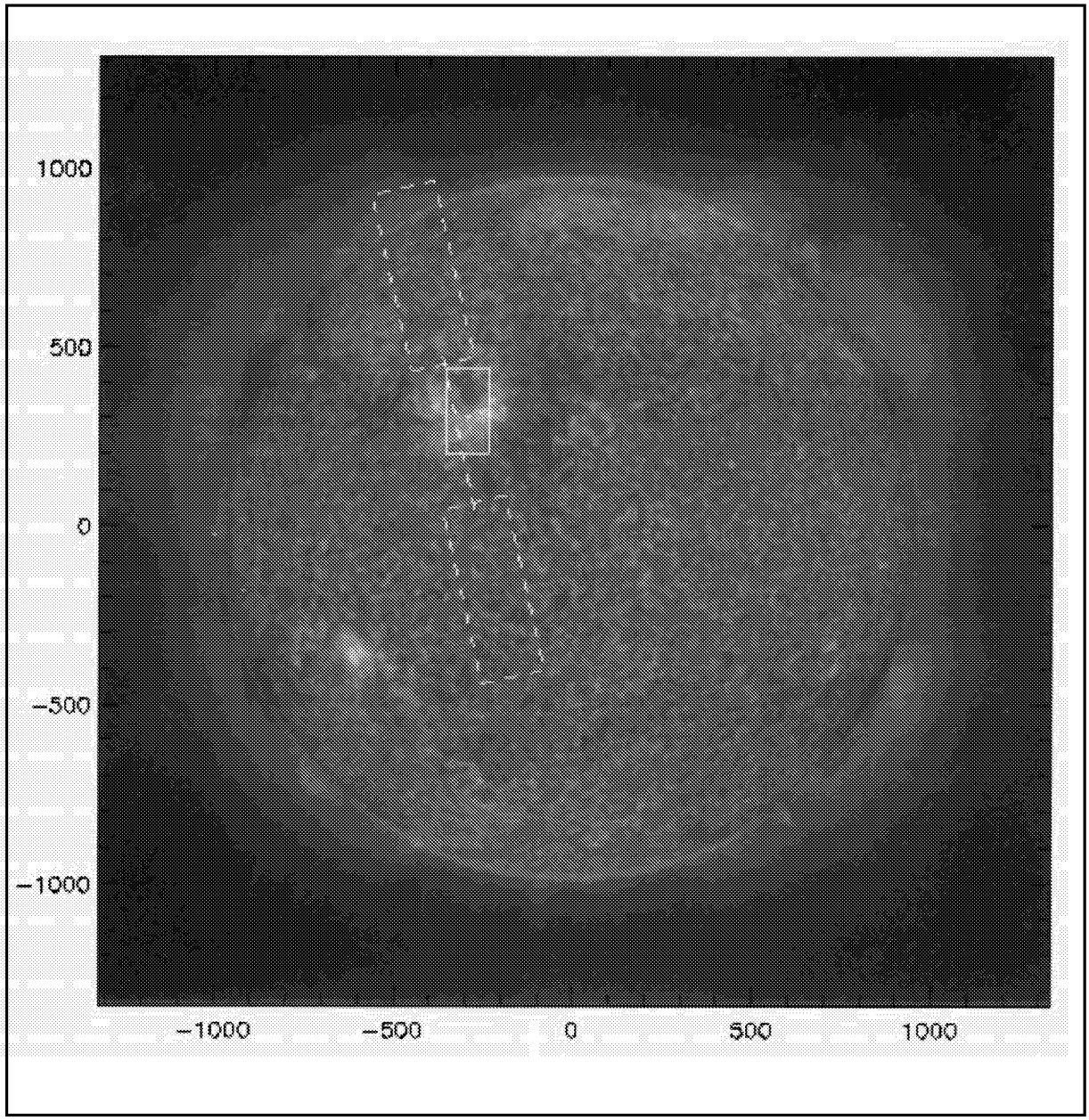

Figure 24. SERTS pointing position 2 (dotted line) of aperature showing slit over active region. Small box is CDS coverage of same active region.

ACRONYM LIST

A/D	Analog to Digital
ASCL	Automated SPARCS Command Link
BESSY	Synchrotron Radiation Source
CCD	Charge Coupled Device
CDS	Coronal Diagnostic Spectrometer (on SOHO)
DAT	Design, Assembly and Test
EIT	EUV Imaging Telescope (on SOHO)
EUV	Extreme Ultraviolet
FO	Fiber Optic
FWC	Full Well Capacity
GSE	Ground Support Equipment
GSFC	Goddard Space Flight Center
Hα	Hydrogen-Alpha Spectral Line (6563 A)
HVPS	High Voltage Power Supply
IDL	Interactive Data Language
I/F	Interface
IGN	Igniter Housing
LISS	Lockheed Intermediate Sun Sensor
LN_2	Liquid Nitrogen
MASS	Miniture Acquisition Sun Sensor
NASA	National Aeronautics and Space Administration
MCP	Microchannel Plate
MCPT	Microchannel Plate Tube
MOI	Moments of Inertia
OGIVE	Curved Shape Nose Cone
ORSA	OGIVE Recovery System Assembly
PTB	Physikalisch Technische Bundesansalt (Berlin)
PWR	Power
RAM	Random Access Memory
RAL	Rutherford Appleton Laboratory
S-19	Boost Guidance System
SERTS	Solar Extreme Ultraviolet Rocket Telescope and Spectrograph
SOHO	Solar and Heliospheric Observatory
SPARCS	Solar Pointing Attitude Rocket Control System
T & E	Test & Evaluation
TBD	To be determined
TLM	Telemetry
TM LOS	Telemetry Loss of Signal
TNT	Theoretical Nose Tip
VAB	Vehicle Assembly Building
WSMR	White Sands Missile Range

BIBLIOGRAPHY

Brosius, J.W., J.M. Davila, and R.J. Thomas, 1998: Solar Active Region and Quiet–Sun EUV Spectra from SERTS–95. *Astrophysical Journal*, (in press).

Brosius, J.W., J.M. Davila, and R.J.Thomas, 1998: Calibration of the SERTS-95 Spectrograph from Iron Line Intensity Ratios. *Astrophysical Journal,* **497**, L113–L116.

Brosius, J.W., J.M. Davila, R.J. Thomas, and B.C. Monsignori-Fossi, 1996: Measuring Active and Quiet Sun Coronal Plasma Properties with EUV Spectra from SERTS. *Astrophysical Journal Supplement Series,* **106**, 143–164.

Brosius, J.W., J.M. Davila, R.J. Thomas, and S.M. White, 1997: Coronal Magnetography of a Solar Active Region Using Coordinated SERTS and VLA Observations. *Astrophysical Journal,* **488**, 488–498.

Brosius, J.W., J.M. Davila, R.J. Thomas, and W.T. Thompson, 1994: Solar Coronal Temperature Diagnostics Using Emission Lines from Multiple Stages of Ionization of Iron. *Astrophysical Journal,* **425**, 343–347.

Brosius, J.W., J.M. Davila, R.J. Thomas, B.C. Monsignori-Fossi, and J.L.R. Saba, 1996: Measurements of Active and Quiet Sun Coronal Plasma Properties with SERTS EUV Spectra. *Proceedings IAU*, **153**. In: *Magnetodynamic Phenomena in the Solar Atmosphere* . Uchida, Kosugi, & Hudson, Eds. Tokyo, 421–422.

Brosius, J.W., J.M. Davila, R.J. Thomas, J.L.R. Saba, H. Hara, and B.C. Monsignori-Fossi, 1997: The Structure and Properties of Solar Active Regions and Quiet-Sun Areas Observed in Soft X-Rays with Yohkoh/SXT and in the EUV with SERTS. *Astrophysical Journal* , **477**, 969–981.

Brosius, J.W., J.M. Davila, R.J. Thomas, S.D. Jordan, and B.C. Monsignori-Fossi, 1996: Solar EUV Spectroscopy with SERTS: Measurements of Active and Quiet Sun Properties. In: *UV & X-ray Spectroscopy of Astrophysical and Laboratory Plasmas*. Yamashita & Watanabe, Eds. Universal Academy Press, 83-88.

Brosius, J.W., J.M. Davila, W.T. Thompson, R.J. Thomas, G.D. Holman, N. Gopalswamy, S.M. White, M.R. Kundu, and H.P. Jones, 1993:*Ap. J.* **411, 410**.

Davila, J.M., R.J. Thomas, W.T. Thompson, R.A.M. Keski-Kuha, and W.M. Neupert, 1993: *First Flight of an Extreme-Ultraviolet Spectrometer with Multilayer Grating, UV and X-ray Spectroscopy of Laboratory and Astrophysical Plasmas*. Silver and Kahn, Eds. Cambridge Univ. Press, 301-304.

Falconer, D.A., 1994: Relative Elemental Abundance and Heating Constraints determined for the Solar Corona from SERTS measurements. Ph.D. Thesis, *NASA Technical Memorandum 104616*.

Falconer, D.A., S.D. Jordan, J.W. Brosius, J.M. Davila, R.J. Thomas, V. Andreatta, and H. Hara, 1998: Using Strong Solar Coronal Emission Lines as Coronal Flux Proxies. *Solar Physics,* **180**,179–191.

Hollandt, J., M. Kühne, M.C.E. Huber, and B. Wende, 1996: Source Standards for the Radiometric Calibration of Astronomical Telescopes in the VUV Range. *Astron. Astrophy. Suppl. Ser.,* **115,** 561–572.

Jordan, S.D., 1994: Line Formation and Intensity Enhancement of the He II 304A Line in the Solar Atmosphere. Proceedings *IAU* **144**, *Solar Coronal Structures* . Rusin, Heinzel, and Vial, Eds. 415-420.

Jordan, S.D., W.T. Thompson, R.J. Thomas, and W.M. Neupert, 1993: Solar Coronal Observations and Formation of the He II 304A Line. *Astrophysical Journal* , **406**, 346–349.

Kelly, R.L. and L.J. Polumbo, 1973: Atomic and Ionic Emission Lines Below 2000 Å. Naval Research Laboratory, *Report 7599*, Washington, D.C.

Keski-Kuha, R.A.M., R.J. Thomas, and J.M. Davila, 1991: Rocket Flight of a Multilayer Coated High-Density EUV Toroidal Grating. *SPIE*: Multilayer and Grazing Incidence X-Ray/EUV *Optics* **1546**, 614-623.

Leviton, D.B., G.A. Wright, R.J. Thomas, J.M. Davila, and G.L. Epstein, 1995: Performance Comparison of Two Wolter Type-II Telescopes in the Far Ultraviolet. *Applied Optics,* **34**, 6459–6464.

Neupert, W.M., G.L. Epstein, R.J. Thomas, and W.T. Thompson, 1992: An EUV Imaging Spectrograph for High-Resolution Observations of the Solar Corona. *Solar Physics* **137**, 87-104.

Neupert, W.M., J.W. Brosius, R.J. Thomas, and W.T.Thompson, 1992: *Ap. J. (Let)* **392**, L95.

Ruggieri, D.J., 1972: Microchannel Plate Imaging Detectors. *IEEE Transactions on Nuclear Science,* **19**, No. 3-6, 74–84.

Swartz, M., G.L. Epstein, and R.J. Thomas, 1988: A Research Amplifying Image Detector (RAID) for the Study of Dynamic Solar Phenomena. *NASA/GSFC Report X-682-88-2.*

Thomas, R.J., C.E. Condor, J.P. Haas, D.L. Linard III, M.Swartz, B.J. Kent, and J. Hollandt, 1997: Absolute Radiometric Calibration of SERTS. *Bulletin American Astronomical Society*, **29**, 1321.

Thomas, R.J., R.A.M. Keski-Kuha, W.M. Neupert, C.E. Condor, and J.S. Gum, 1991: Extreme-Ultraviolet Performance of a Multilayer Coated High-Density Toroidal Grating. *Applied Optics* **30**, 2245-2251.

Thomas, R.J., W.M. Neupert, and W.T. Thompson, 1993: *Calibrated Solar EUV Spectra from SERTS, UV and X-ray Spectroscopy of Laboratory and Astrophysical Plasmas* (Eds: Silver & Kahn, Eds. Cambridge Univ. Press, 391-394; and *Physics of Solar and Stellar Coronae*. Linsky and Serio, Eds. Kluwer Acad. Pub, 195-198.

Thomas, R.J. and W.M. Neupert, 1994: Extreme Ultraviolet Spectrum of a Solar Active Region from SERTS. *Astrophysical Journal , Supplement Series* **91**, 461–482.

Thomas, R.J. and W.M. Neupert, 1995: Extreme Ultraviolet Spectrum of a Solar Active Region from SERTS. *ASP Conference Series* 81, 105–106.

Thompson, W.T., A.I. Poland, M. Swartz, D.B. Leviton, L.J. Payne, O.H.W. Siegmund, and D. Marsh, 1994: Characterization of the SOHO CDS Normal Incidence Detector. *EOS Transactions American Geophysical Union*, **75**, *#16/suppl.,* 257.

Thompson, W.T., A.I. Poland, O.H. Siegmund, M. Swartz, D.B. Leviton, L. J. Payne, Measurements of an Intensified CCD Detector for Solar Heliospheric Observatory. *SPIE*, **1743**.

Thompson, W.T., W.M. Neupert, S.D. Jordan, H. Jones, R.J. Thomas, and B. Schmieder, 1993: Correlation of He II Lyman-Alpha with He I 10830 Å, and with Chromospheric and EUV Coronal Emission. *Solar Physics* **147**, 29–46.

Thompson, W.T. and M. Swartz, 1990: Research Amplifying Imaging Detector. *NASA Research and Technology Report.*

Young, P.R. and H.E. Mason, 1996: EUV Density Diagnostics in Solar and Stellar Spectra. *ASP Conference Series* , **109**, 301–302.

APPENDICES

CONTACT INFORMATION

A. E-MAIL ADDRESSES – CODE 682

Brosius@stars.gsfc.nasa.gov
Davila@lindsay.gsfc.nasa.gov
Jordan@stars.gsfc.nasa.gov
MSwartz@stars.gsfc.nasa.gov
Thomas@jet.gsfc.nasa.gov

B. SUPPORT PERSONNEL AT WALLOPS FLIGHT FACILITY AND WHITE SANDS MISSILE RANGE

Wallops Flight Facility

Person	Organization	Function
W. Frank Lau	Sounding Rocket and Range Management Branch	Project Manager and Payload Manager
Charles Lipsett	"	Mechanical Structures
Maria Cabauero	"	Flight Performance

White Sands Missile Range

Person	Organization	Function
Lockheed Martin Technical Operations (LMTO) SPARCS Program:		
C.W. Welch	LMTO/SPARCS	Manager
Becky Grzelachowski	LMTO/SPARCS	Administration
Richard N. Rakoff	LMTO/SPARCS	Mission Coordinator, s-19
Shelby C. Elborn	LMTO/SPARCS	Telemetry
Jesus E. Martinez	LMTO/SPARCS	SPARCS ACS
Carlos Martinez	LMTO/SPARCS	Command Link
Bryan Traylor	LMTO/SPARCS	Command Link
Bruce Howard	LMTO/SPARCS	SPARCS Elect. Tech.
Ken Starr	LMTO/SPARCS	TM Elect. Tech.
Al Lambert	LMTO/SPARCS	Mechanical & Pneumatics
Paul Harmon	LMTO/SPARCS	Mechanical & Pneumatics
New Mexico State University Physical Science Laboratory (NMSU/PSL):		
J. Allan Baker	NMSU/PSL	Mgr., PSL TM Support Group/VAB
Diana Vigil	NMSU/PSL	Secretary
Marcos Quinones	NMSUIPSL	ORSA & Ign. Hsng./Mech.
David Garcia	NMSU/PSL	ORSA & Ign. Hsng.
Gary Carr	NMSUIPSL	ORSA & Ign. Hsng./Landlines
Debra Asbury	NMSU/PSL	TM Ground Station/VAB
Bill Ludwig	NMSU/PSL	TM Ground Station/VAB
Anthonette Alejandrez	NMSU/PSL	TM Ground Station/VAB
Bob Braithwaite	NMSU/PSL	TM Ground Station/VAB

Gerald Gregg	NMSUIPSL	TM Ground Station/VAB
Troy Gammel	NMSU/PSL	TM Ground Station/VAB
Garen Saulsberry	NMSU/PSL	Sta. Mgr./TM Ground Station/N2OO
Tim Hess	NMSU/PSL	TM Ground Station/NOO
Rodolfo Ortega	NMSU/PSL	TM Ground Station/N200
Lupe Archuleta	NMSU/PSL	TM Ground Station/N2OO
Mark Stoner	NMSU/PSL	TM Ground Station/N200
Naval Air Weapons Center (NAWCWPNS), Research Rockets Division:		
Tom Gonzales	NAWCWPNS/*NAVY*	Chief, Research Rockets Div.
Bill Landers	NAWCWPNS/NAVY	Launch Officer
Lydia Valle	NAWCWPNS/NAVY	Secretary
pol Scot McPartland	NAWCWPNS/NAVY	Launch Assistance
Pol Guy Budschlick	NAWCWPNS/NAVY	Launch Assistance
Johnny Grzelachowski	NAWCWPNS/NAVY	NAVY Scheduler
Jose Guerrero	Tritek	Launch Assistance
Jack CrouchD Jr.	Tritek	Launch Assistance
Richard Evavold	Tritek	Bldg. 300 Coordinator
Ted Powell	SWTDS/Tritek	Financial Data for NASA and Data Transport

REPORT DOCUMENTATION PAGE

Form Approved
OMB No. 0704-0188

1. AGENCY USE ONLY *(Leave blank)*	2. REPORT DATE	3. REPORT TYPE AND DATES COVERED
	February 1999	Technical Publication

4. TITLE AND SUBTITLE
The SERTS–97 Rocket Experiement to Study Activity on the Sun: Flight 36.167–GS on 1997 November 18

5. FUNDING NUMBERS
Code 682

6. AUTHOR(S)
Marvin Swartz, Charles E. Condor, Joseph M. Davila, J. Patrick Haas, Stuart D. Jordan, David L. Linard, Joseph J. Miko, I.Carol Nash, Joseph Novello, Leslie J. Payne, Thomas B. Plummer, Roger J. Thomas, Larry A. White, Jeffrey W. Brosius, and William T. Thompson

7. PERFORMING ORGANIZATION NAME(S) AND ADDRESS (ES)
Laboratory for Astronomy and Solar Physics
Goddard Space Flight Center
Greenbelt, Maryland 20771

8. PEFORMING ORGANIZATION REPORT NUMBER
99B00010

9. SPONSORING / MONITORING AGENCY NAME(S) AND ADDRESS (ES)
National Aeronautics and Space Administration
Washington, DC 20546-0001

10. SPONSORING / MONITORING AGENCY REPORT NUMBER
TP–1999–208640

11. SUPPLEMENTARY NOTES
J. Brosius: Raytheon STX Corporation, Lanham, Maryland
William T. Thompson: Space Applications Corporation, Largo, Maryland

12a. DISTRIBUTION / AVAILABILITY STATEMENT
Unclassified–Unlimited
Subject Category: 89
Report available from the NASA Center for AeroSpace Information, 7121 Standard Drive, Hanover, MD 21076-1320. (301) 621-0390.

12b. DISTRIBUTION CODE

13. ABSTRACT *(Maximum 200 words)*

This paper describes mainly the 1997 version of the Solar EUV Rocket Telescope and Spectrograph (SERTS–97), a scientific experiment that operated on NASA's suborbital rocket flight 36.167–GS. Its function was to study activity on the Sun and to provide a cross calibration for the CDS instrument on the SOHO satellite. The experiment was designed, built, and tested by the Solar Physics Branch of the Laboratory for Astronomy and Solar Physics at the Goddard Space Flight Center (GSFC). Other essential sections of the rocket were built under the management of the Sounding Rockets Program Office. These sections include the electronics, timers, IGN despin, the SPARCS pointing controls, the S–19 flight course correction section, the rocket motors, the telemetry, ORSA, and OGIVE. Documents describing these sections and their operation can be acquired by contacting Frank Lau, Payload Manager, Code 810, at NASA/GSFC, Wallops Flight Facility, Wallops Island, Virginia 23337. There were many people at White Sands Missile Range and Wallops Flight Facility who worked on the payload and rocket sections listed above; they all were instrumental in the success of the flight. Their names are listed in the Appendix.

14. SUBJECT TERMS
Solar EUV Rocket Telescope and Spectrograph (SERTS), Sun, Rocket, SOHO, Configuration

15. NUMBER OF PAGES
48

16. PRICE CODE

17. SECURITY CLASSIFICATION OF REPORT	18. SECURITY CLASSIFICATION OF THIS PAGE	19. SECURITY CLASSIFICATION OF ABSTRACT	20. LIMITATION OF ABSTRACT
Unclassified	Unclassified	Unclassified	UL